Desalination of Produced Water via Gas Hydrate Formation and Post Treatment

Jing Niu

Thesis submitted to the Faculty of the
Virginia Polytechnic Institute and State University
in partial fulfillment of the requirement for the degree of

Master of Science
in
Mining and Minerals Engineering

Roe-Hoan Yoon, Chair
Gregory T. Adel
Gerald H. Luttrell
Richard D. Gandour

April 19th 2012
Blacksburg, Virginia

Keywords: desalination, gas hydrate, centrifuge, filtration

Desalination of Produced Water via Gas Hydrate Formation and Post Treatment

by

Jing Niu

Abstract

This study presents a two-step desalination process, in which produced water is cleaned by forming gas hydrate in it and subsequently dewatering the hydrate to remove the residual produced water trapped in between the hydrate crystals. All experiments were performed with pressure in the range of 450 to 800psi and temperature in the range of -1 to 1°C using CO_2 as guest molecule for the hydrate crystals. The experiments were conducted using artificial produced waters containing different amounts of NaCl, $CaCl_2$ and $MgCl_2$ at varying temperature (T) and pressure (P). The results are presented as functions of %Reduction of difference chemical elements, CO_2 requirements and applied T and P conditions.

The impact of dewatering techniques, including centrifuge and filtration process, on gas hydrate solid product is studied. The results showed that over 99% of dissolved NaCl and $MgCl_2$ can be removed from artificial saline water in laboratory experiments. This was achieved in a process involving a single-stage hydrate formation step, followed by a single-step solid-liquid separation (or dewatering). The results also show that the %Reduction (percentage of the concentration decrease) of artificial produced water increases with centrifugation time and rotational speed (rpm). The %Reduction was increased considerably after hydrate crystals were crushed and filtered, indicating that the artificial process water was entrapped in between the hydrate crystals. It was found also that the finer the particle size, the higher the extent of salt removal. In general, filtration was a better than centrifugation for the removal of TDS (Total Dissolved Solids).

Acknowledgement

First and foremost, I would like to acknowledge my advisor, Dr. Roe-Hoan Yoon, for his support and guidance throughout my two years study in Virginia Tech. I would like to express my appreciation to him for his help both for my research life and my personal life in Blacksburg. During this period, I have learned a lot from Dr. Yoon about how to conduct research projects, how to think, how to write. I also thank Dr. Gregory Adel, Dr. Gerald Luttrell and Dr. Gandour who served as my thesis committee member for their suggestions on my research works.

I sincerely appreciate to Dr. Jialin Wang for his guidance and instruction in gas hydrate formation and Lei Pan for his patient instruction and guidance in experimental methods. Especially, I would like to thank Mr. Zuoli Li and Juan Ma who solved my titration problem in testing ion concentration.

I would like to express my appreciation to Yongkoo Seol for his discussion on technical problems on filtration process. Also I want to express my sincere gratitude to Dr. Jongho Cha for his discussion on gas hydrate formation kinetic and equilibrium process.

I would like to thank past and present members in Center of Advanced Separation Techniques (CAST), Chris Hull, Kirsten Titland and Dr. Jinming Zhang for their support and help.

Last but not least, I would like to express my deepest gratitude to my parents for their selfless love and support. Without their love and support, I would not have my accomplishment.

TABLE OF CONTENT

Table of Figures

List of Tables

Chapter 1 Introduction

1.1 General Background

The 20th century has experienced a rapid global population increase and along with it, an explosive growth of potential water shortage problems. This shortage can be partially attributed to limited natural resources and increased industrial activities. To resolve the water scarcity problems in many regions, seawater is no longer merely a marginal water resource but a commercial option for securing water supplies. Desalination applications are not limited to seawater; brackish water, river water and wastewater also apply.

Desalination of saline water must be regarded seriously in the above circumstances. Desalination technologies can be classified by their separation mechanism into membrane based and thermal desalination. In membrane desalination, water diffuses through a membrane, while salts are almost completely retained, i.e., reverse osmosis. Thermal desalination separates salt from water by evaporation and condensation, i.e., distillation.

Reverse osmosis (RO) membrane desalination is a well-established membrane-based water desalination technology. It has the advantages of high efficiency and low energy cost, however, the process consumes a large amount of fresh water due to the low backpressure. As a result, only 5-15 percent of the water entering the system can be recovered. [7] Due to its membrane construction of fine pores, reverse osmosis not only removes contaminants that may be present in the water, it strips many of the good, healthy minerals from the water as well. Reverse Osmosis water is so chemically unstable and acidic that many countries restrict water filtered via reverse osmosis from being reintroduced into copper pipe due to its corrosiveness of the copper. This also has implications for reverse osmosis filtration systems that use steel storage tanks, as the acidity of the water can lead to the steel rusting over time and contaminating the post-filter water.

Another widely used desalination technology is the distillation method. All distillation techniques are based on a similar working principle. The water and the dissolved gases in it are volatile when boiling saline water, while the minerals and dissolved salts do not

evaporate easily unless with boiling temperatures are above 300 °C. Single stage distillation, multi-stage distillation and other kinds of new distillation techniques have been developed. [8] The techniques above both address the problems in the treatment of high salinity water, like produced water from shale gas industry. This way, clathrate hydrate crystallization has been reconsidered as a potential unit operation for high salinity water desalination.

Gas hydrates (clathrate hydrates) are crystalline solid structures consisting of water and small molecules, gas or liquid, such as CO_2, N_2, CH_4, *et al.* which are formed under conditions of specific temperature and pressure. It is now obvious that clathrate hydrate are non-stoichiometric compounds and different from ice which has a hexagonal structure. The majority of gas hydrates are known to form three typical hydrate crystal structures, structure I (sI), structure II (sII), and structure H (sH) [9] . **Figure 1.1** shows the different hydrate structures and their associated cage type: sI comprises two different cage types, a small pentagonal dodecahedral cage, denoted 5^{12} (contains 12 pentagonal faces on the cage), and a large tetrakaidecahedral cage, denoted $5^{12}6^2$ contains 12 pentagonal and 2 hexagonal faces on the cage). sII also includes the small 5^{12} cage in addition to a large hexacaidecahedral cage, denoted $5^{12}6^4$ (contains 12 pentagonal and 4 hexagonal faces on the cage). Structure H is composed of the small 5^{12} cage, a mid-sized $4^3 5^6 6^3$ cage (contains 3 square, 6 pentagonal, and 3 hexagonal faces on the cage), and a large icosahedral cage, denoted $5^{12}6^8$ (contains 12 pentagonal and 8 hexagonal faces on the cage). The type of structure formed depends primarily on the size of the guest molecule; i.e., methane fits into both the small and large cages of sI, whereas propane is too large to fit into the large cage of sI but can fit into the large cage of sII and therefore forms sII. Gas hydrates found in oil and gas pipelines are mainly sII because natural gas contains methane with small amounts of larger hydrocarbon molecules such as propane and isobutane. Conversely, the majority of naturally occurring deposits of gas hydrates are sI because they are composed of methane (from biogenic sources) and do not contain heavier hydrocarbons. Exceptions are thermogenic gas hydrate deposits that contain heavier hydrocarbons and therefore are formed from sII and in rarer cases sH. In a gas hydrate structure, water molecules consist of cavity, and usually each cavity includes one gas or liquid molecule inside.

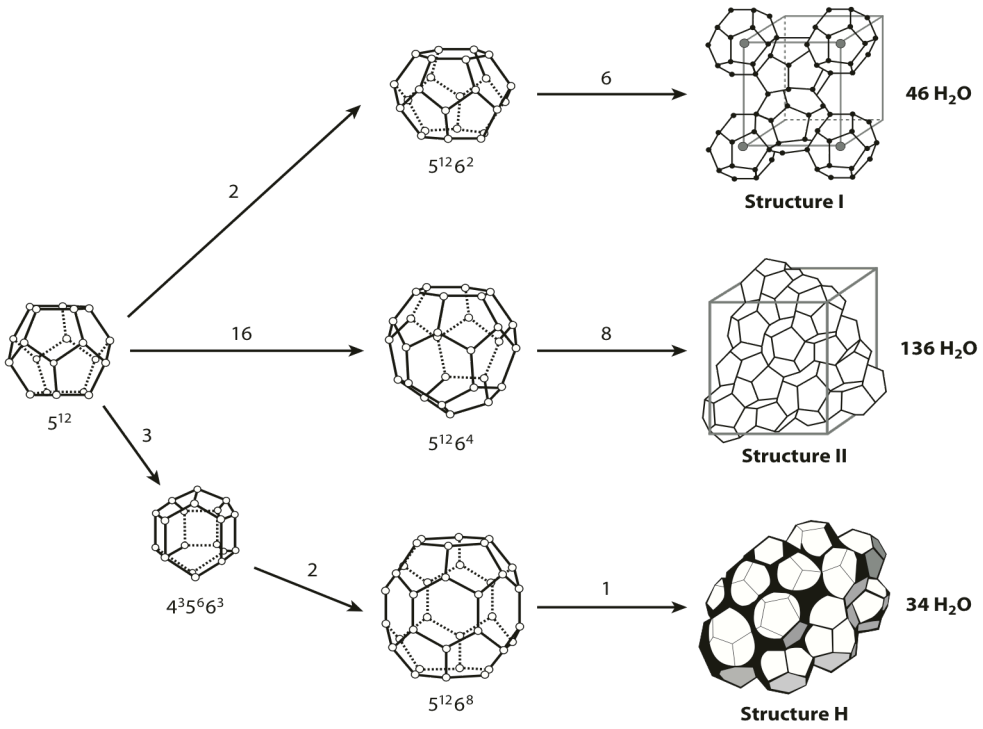

Figure 1.1 Different types of gas hydrate

In principle, CO_2 hydrate is formed with pure water, thereby excluding dissolved impurities. After gas hydrate formation, we assume there may be brine ions trapped in between CO_2 hydrate. In the present work, we used artificial brine solutions of NaCl, $MgCl_2$ and $CaCl_2$ with varying concentrations. All CO_2 hydrates were formed at 1°C and 600–700psi. Gas hydrate formation-centrifuge and gas hydrate formation-filtration processes were operated, and desalination %Reductions of different experiments operations were calculated and compared.

1.2 Literature Review

Gas hydrate has been applied in several fields, including flue gas adsorption, green house gas or hazardous gas storage, gas separation, desalination, *etc.* thermodynamic, kinetic process, and phase equilibrium condition measurement during the gas hydrate formation process.

Desalination by Freezing

During the freezing process, only water molecules can construct ice crystal and salts are excluded under controlled conditions. Before the entire mass of water has been frozen, the mixture is usually washed and rinsed to remove salts in the remaining water or adhering to the ice. [10]

Youssef Mandri et al. [11] studied the sweating step in the seawater desalination process by indirect freezing. The whole process of desalination involves a freezing step, followed by a purification of the ice layer by sweating. They successfully reduced an ice layer of salinity from 35g/kg to lower than 0.5g/kg within 23h, obtaining a desalination efficiency of 86%. They concluded that progressive increase of the sweating temperature does not seem to bring more salinity away from ice layer.

Cong-shuang Luo et al.[12] worked on factors affecting the quality of ice crystal during the freezing concentration for the brackish water by using the method of crushing ice and centrifugation. From their experiments, it was almost impossible to obtain pure ice crystals with the freezing method only, because during the growth that solution was trapped in ice in the form of brine pockets according to Ebert et al.[13] . Crushing ice can lead to the breakage of this structure and release brine.

Lubos Vrbka and Pavel Jungwirth[14] studied the molecular dynamics of brine rejection from freezing salt solutions. They observed that the system freezes as neat ice by expelling ions into a higher brine concentration region, where ions can sometimes be trapped inside the ice crystal and incorporated further water molecules into the ice lattice slower.

Khhoudir Medjani[15] believed in the existence of brine pocket during the freezing of NaCl-H_2O compound. They observed the interface between the ice and liquid, revealing that the liquid is trapped inside the mushy zone (a place where liquid and ice coexist) in the form of pockets as a result of necking of the interfacial tubes as the ice grows.

Freeze-melting process requires much less energy than evaporation/distillation process and minimizes the capital cost because many inexpensive plastics or low cost materials

can be utilized at low temperature. [16] However, It has not achieved commercial success because of the complexity of the process and higher cost in total.

Phase Equilibrium in Gas Hydrate Formation

Usually, three major methods are used in gas hydrate phase equilibrium measurement, Gibbs phase rule, Duhem's theorem and Van Poolen. Juan G. Beltran, Hallvard and Phillip [17] summarized the Gibbs phase rule in measuring techniques in gas hydrate equilibrium. Pure hydrate system and divariant or multicomponent hydrate system are studied.

In the pure hydrate system [18] , only one variable needs to be controlled to search for equilibrium. Some laboratories prefer to manipulate temperature while others tend to control pressures. In a divariant hydrate system, three variables including pressure and temperature need to been provided and plotted, and verification need to be done through comparison [19].

J.- M. Herri, A. Bouchemoua, *et al.*[20] studied the gas hydrate equilibrium for CO_2-N_2 and CO_2-CH_4 mixtures. They analyzed the gas mixtures with a gas chromatography to obtain the exact composition of each gas and calculated gas composition in different phases through the gaseous component mass balance

Xiao-Sen Li et al. [21-23] studied the effect of tetrabutyl ammonium bromide (TBAB) on equilibrium of CO_2-H_2 mixture hydrate formation. They confirmed as Hashimoto et al. and Aladko et al. reported that type B TBAB hydrate formed preferentially with mole fraction less than 1.4%, while type A TBAB hydrate is more thermodynamically stable with mole fraction larger than 1.4%. From experiments they found that the addition of TBAB reduces pressure in hydrate formation considerably, TBAB additive make a larger reduction of the equilibrium formation pressure comparing to THF and CP. They obtained gas separation efficiency by reducing CO_2 mole fraction from 39.2 to 18%.

Kinetic Formation of Gas hydrate

Junshe Zhang and Jae W. Lee [24] worked on enhancing kinetic formation of CO_2 hydrate by adding cyclopentane (CP). They found that increasing the amount of CP leads

to an increase of both the water conversion and CO_2 recovery, while decreasing the ratio of CO_2 entrapped in sI hydrate to that in sII hydrate [25] . When they increased the formation water supply from 100 to 200cm^3, the water conversion and CO_2 growth rate both decreased for the first charge of CO_2, and with more gas hydrate formed. They also considered that the driving force of hydrate formation is the highest near vessel wall which cause the gas hydrate to grow along the wall, and more hydrate accumulate as a porous structure at this position and draw water from bulk water by the capillary force.

Matthew A. Clarke and P.R. Bishnio [28] worked on the intrinsic kinetics of CO_2 hydrate formation by using in situ particle size analysis with a focused beam reflection method (FBRM). The starting point of nucleation was observed when the small particles number decreased immediately while the large particles number began to grow.

J. S. Zhang, et al. [29] found there is no clear relation between SDS addition amount and induction time. The promoting effects of SDS on hydrate nucleation was confirmed, though increasing SDS may inhibit initial hydrate nucleation due to the fact adding electrolyte concentration decrease water activity. They got that SDS can prevent the agglomeration of hydrate particles, which contribute to increasing particle numbers over time for a given nucleation rate at the start of hydrate growth.

Seong-Pil Kang and Yutaek Seo [30] formed methane and carbon dioxide hydrate in silica gel pores instead of traditional mechanical stirring method. They figured out that methane hydrate formation rate is not dependent on the pore size, and for carbon dioxide hydrate there exists an optimal pore size for the hydrate formation rate. Though hydrate formed from porous silica takes longer formation time and has lower initial formation rate than traditional methods, they accomplished remarkable cage occupancy and helped to remove expensive mechanical agitation.

Masayoshi Takahashi et al. [31] found the possibility of applying shrinking microbubble on the gas hydrate formation due to their large surface area, very long stagnation and a pressurized interior gas. They pointed out that microbubble can change the nucleation conditions because of its excellent gas-dissolving capacity. Hideo Tajima, et al. [32]

thought about the possibility to replace traditional stirring vessels with a kinetic-type static mixer in formation of CO_2 hydrate continuously.

Thermodynamic Properties Improvement in Gas Hydrate Formation

Atle Svandal, et al. [32] focused on thermodynamic properties of the $H_2O/CO_2/CH_4$ system, especially the interface thermodynamics. They considered interfacial thickness and free energy to derive kinetic and thermodynamic properties. Their investigation into bulk CO_2 hydrate and water system showed the hydrogen bonds per water molecule is 1.65 for hydrate water, while 1.39 for liquid water, and thus they expected that the interface Gibbs free energy for this hydrate system is close to that of ice-water system (γ=29.1±0.8 mJ/m^2).

Angel Martin and Cor J. Peters [2] modified the fugacity-based Van der Waals-Platteeuw model of Klauda and Sandler [33] . From substitution of thermodynamic model they modified, they figured out that the lattice distortion depends only on the occupancy of the large cavity by THF. Also they got that neither large nor small cavity occupancies has variations with the initial concentration of THF in the mixture, changing the initial addition of THF can only lead to the amount of hydrate formed.

Instrumental Techniques in Analyzing Gas Hydrate Formation

A series of advanced instrumental techniques are needed to observe the gas hydrate formation, as well as the structures and properties of different kinds gas hydrate[34] .

Y. Rojas and X. Lou [35] summarized some modern instrumental analyses and their corresponding basic physical science principles and the gas hydrate properties that each method can characterize. Robert W. Hennig, Arthur J. Schultz, et al. [36] investigated the formation of CO_2 hydrate in the use of time-of-flight neutron powder diffraction at temperature range of 230 to 290K, and a pressure of 900psi. They found that peaks corresponding to ice slowly disappeared, while hydrate peaks intensity increased when the sample reached 275.6K. Diffraction peaks of indicating ice disappeared completely at 276.4K, while the diffraction peaks of hydrate number appeared and began to increase. They also certificated the phenomenon that the rate-limiting step of the process after

approximately 20% conversion is the diffusion of CO_2 molecules through the layer of hydrate [37] , in agreement with the assumption [1] that the slow transport of CO_2 molecules across the growing solid hydrate layer may cause the slower CO_2 hydrate growth rate in a water drop covered with a thin film of CO_2 hydrate [1] .

Igor L, Christopher I. Ratcliffe, et al. [2] used 1H NMR (Nuclear Magnetic Resonance) microimaging techniques to examine hydrate-coated ice particle as a function of temperature from 250 to 276K. From images captured by NMR, they figured out that ice inside the hydrate, though may not be easily observed by monitoring temperature and pressure, are able to melt. They also observed that conversion from ice to hydrate is stopped where the volume required inside the shell increased as shown in **Figure 1.2**, which in agreement with the Pilling-Bedworth rule believing that the surface reaction

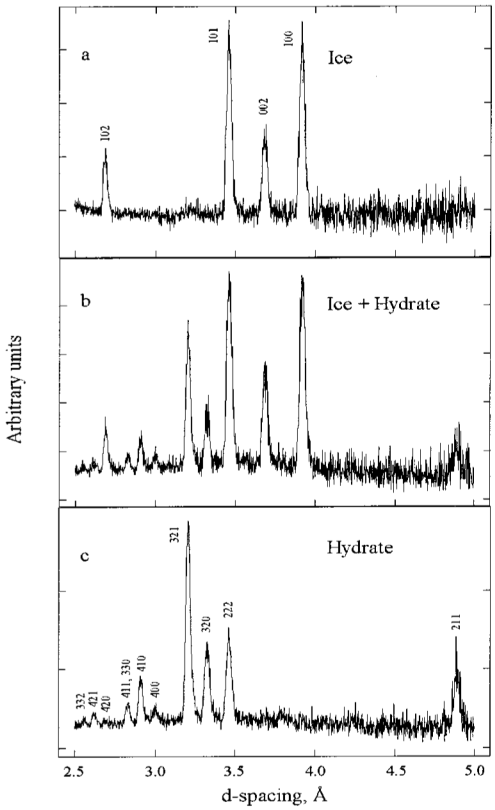

Figure 1.2 Transformation of D_2O ice to CO_2 hydrate: (a) ice at 263 K before adding CO_2; (b) mixture of ice and CO_2 hydrate at 263 K and 900 psi; (c) CO_2 hydrate at 276.4 K and 900 psi. The noisy background is due to the short collecting times of 15 min per histogram. [6]

should result in a dense surface-layer that ultimately limits the reaction.

Carolyn A. Koh and Jeffery L. Savidge [3] used energy-dispersive diffraction in capturing the crystalline structural dynamics of carbon dioxide and propane hydrate structures during formation. They confirmed the sI structure of CO_2 hydrate and sII of propane hydrate.

T Komai, T Kawamura, et al. observed in situ gas hydrate behavior under high pressure with Raman spectroscopy. At first, they tested CH_4 hydrate and got the hydrate number in the range of 6.4-6.0, the occupancy ratio in small cages was estimated to be approximately 85-95%, meanwhile, presence of guest gases in large and small cages are both measured and showed by peaks in Raman spectra from **Figure 1.3**. In measurement of CO_2 gas hydrate, they found that gas hydrate formation rate change greatly with temperature, especially in the range between 269 and 275K, suggesting the existence of quasi-liquid water, a type of slightly melting ice that help to promote gas hydrate formation in the gas-solid interface.

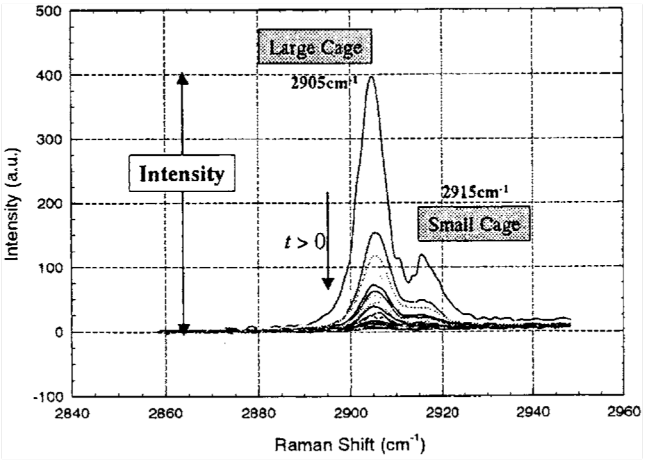

Figure 1.3 Raman shifts in the disassociation of CH_4 gas hydrate [3]

Hydration Energy of Selected Ions

Enthalpy of hydration, which is the amount of energy released when a mole of the ion dissolves in a large amount of water forming a hydrated ion. Hydration energy of selected ions is listed in Figure 1.4.

Hydration Enthalpies of Metal Cations (kJ/mol)

Electronegativity ≤1.5			Electronegativity ≥1.5		
Ion	Radius	ΔH_{hyd}	Ion	Radius	ΔH_{hyd}
+1 Ions					
Cs	181	−263			
Rb	166	−296	Tl	164	−326
K	152	−321			
Na	116	−405	Ag	129	−475
Li	90	−515	Cu	91	−594
H		−1091			
+2 Ions					
Ra		−1259			
Ba	149	−1304			
Sr	132	−1445	Pb	133	−1480
No	124	−1485	Sn		−1554
Ca	114	−1592	Cd	109	−1806
			Cr	94	−1850
			Mn	97	−1845
			Fe	92	−1920
			Co	88	−2054
			Ni	83	−2106
			Cu	91	−2100
Mg	86	−1922	Zn	88	−2044
			Be	59	−2487
+3 Ions					
Pu	114	−3441			
La	117	−3283			
Lu	100	−3758	Tl	102	−4184
Y	104	−3620	In	94	−4109
Sc	88	−3960	Ga	76	−4685
			Fe	78	−4376
			Cr	75	−4402
			Al	67	−4660
+4 Ions					
Ce	101	−6489			

Ionic radii are from Table C; hydration enthalpies are taken from J. Burgess, *Metal Ions in Solution*, Ellis Horwood, Chichester, England, 1978, pp. 182–183.

Figure 1.4 Hydration energy of different ion

1.3 Research Objectives

The objective of this project is to demonstrate a potential application of gas hydrate science for the removal of salts and other impurities from the produced water, particularly from those released in the oil and gas industries. In the shale gas industry, typically 20-40% of the frac water flows back to the surface. The flow back water contains various dissolved ions, including Na^+, Ca^{2+}, Mg^{2+}, Ba^{2+}, Fe^{2+}, Cl^- and other ions, and the total dissolved solids (TDS) are in the range of 20,000 to 200,00 in the artificial produced water.

In this project, CO_2 hydrates are formed in a high salinity synthesized produced water, separated from residual interstitial water, and decomposed to obtain cleaner water. In principle, CO_2 hydrates are formed only with pure water, excluding dissolved salts. The CO_2 hydrate is chosen, because they can be readily formed under milder temperature and pressure conditions than other gas hydrates such as nitrogen (N_2) or methane (CH_4).

1.4 References

1 Komai, T., Kawamura, T., Kang, S., Nagashima, K. & Yamamoto, Y. In situ observation of gas hydrate behaviour under high pressure by Raman spectroscopy. *J. Phys.-Condes. Matter* **14**, 11395-11400, doi:10.1088/0953-8984/14/44/488 (2002).

2 Henning, R. W., Schultz, A. J., Thieu, V. & Halpern, Y. Neutron diffraction studies of CO2 clathrate hydrate: Formation from deuterated ice. *J. Phys. Chem. A* **104**, 5066-5071, doi:10.1021/jp0001642 (2000).

3 Antony, A. *et al.* Scale formation and control in high pressure membrane water treatment systems: A review. *J. Membr. Sci.* **383**, 1-16, doi:10.1016/j.memsci.2011.08.054 (2011).

4 Saidur, R., Elcevvadi, E. T., Mekhilef, S., Safari, A. & Mohammed, H. A. An overview of different distillation methods for small scale applications. *Renew. Sust. Energ. Rev.* **15**, 4756-4764, doi:10.1016/j.rser.2011.07.077 (2011).

5 Koh, C. A., Sloan, E. D., Sum, A. K. & Wu, D. T. in *Annual Review of Chemical and Biomolecular Engineering, Vol 2* Vol. 2 *Annual Review of Chemical and Biomolecular Engineering* (ed J. M. Prausnitz) 237-257 (Annual Reviews, 2011).

6 Khawaji, A. D., Kutubkhanah, I. K. & Wie, J. M. Advances in seawater desalination technologies. *Desalination* **221**, 47-69, doi:10.1016/j.desal.2007.01.067 (2008).

7 Mandri, Y. *et al.* Parametric study of the sweating step in the seawater desalination process by indirect freezing. *Desalination* **269**, 142-147, doi:10.1016/j.desal.2010.10.053 (2011).

8 Luo, C. S., Chen, W. W. & Han, W. F. Experimental study on factors affecting the quality of ice crystal during the freezing concentration for the brackish water. *Desalination* **260**, 231-238, doi:10.1016/j.desal.2010.04.018 (2010).

9 Ebert, E. E. & Curry, J. A. an intermediate one-dimensional thermodynamic sea-ice model for investigating ice-atmosphere interactions. *J. Geophys. Res.-Oceans* **98**, 10085-10109, doi:10.1029/93jc00656 (1993).

10 Vrbka, L. & Jungwirth, P. Brine rejection from freezing salt solutions: A molecular dynamics study. *Phys. Rev. Lett.* **95**, doi:10.1103/PhysRevLett.95.148501 (2005).

11 Medjani, K. Numerical simulation of the formation of brine pockets during the freezing of the NaCl - H2O compound from above. *Int. Commun. Heat Mass Transf.* **23**, 917-928, doi:10.1016/0735-1933(96)00074-7 (1996).

12 Ahmad, M. & Williams, P. Assessment of desalination technologies for high saline brine applications - Discussion Paper. *Desalin. Water Treat.* **30**, 22-36, doi:10.5004/dwt.2011.1374 (2011).

13 Beltran, J. G., Bruusgaard, H. & Servio, P. Gas hydrate phase equilibria measurement techniques and phase rule considerations. *J. Chem. Thermodyn.* **44**, 1-4, doi:10.1016/j.jct.2011.08.026 (2012).

14 Sloan, E. D. Clathrate hydrates: The other common solid water phase. *Ind. Eng. Chem. Res.* **39**, 3123-3129, doi:10.1021/ie000574c (2000).

15 Uchida, T. *et al.* Kinetics and stability of CH4-CO2 mixed gas hydrates during formation and long-term storage. *ChemPhysChem* **6**, 646-654, doi:10.1002/cphc.200400364 (2005).

16 Herri, J. M. *et al.* Gas hydrate equilibria for CO(2)-N(2) and CO(2)-CH(4) gas mixtures-Experimental studies and thermodynamic modelling. *Fluid Phase Equilib.* **301**, 171-190, doi:10.1016/j.fluid.2010.09.041 (2011).

17 Xiao-Sen Li, †,‡ Zhi-Ming Xia,†,‡,§ Zhao-Yang Chen,†,‡ Ke-Feng Yan,†,‡ Gang Li,†,‡,§ and Hui-Jie Wu†,‡. <Equilibrium Hydrate Formation Conditions for the Mixtures of CO2 + H2 + Tetrabutyl Ammonium Bromide.pdf>. *J. Chem. Eng* (2010).

18 Sakamoto, J. *et al.* Thermodynamic and Raman spectroscopic studies on hydrogen plus tetra-n-butyl ammonium fluoride semi-clathrate hydrates. *Chem. Eng. Sci.* **63**, 5789-5794, doi:10.1016/j.ces.2008.08.026 (2008).

19 Aladko, L. S., Dyadin, Y. A., Rodionova, T. V. & Terekhova, I. S. Clathrate hydrates of tetrabutylammonium and tetraisoamylammonium halides. *J. Struct. Chem.* **43**, 990-994, doi:10.1023/a:1023698728342 (2002).

20 Zhang, J. S. & Lee, J. W. Enhanced Kinetics of CO(2) Hydrate Formation under Static Conditions. *Ind. Eng. Chem. Res.* **48**, 5934-5942, doi:10.1021/ie801170u (2009).

21 Staykova, D. K., Kuhs, W. F., Salamatin, A. N. & Hansen, T. Formation of porous gas hydrates from ice powders: Diffraction experiments and multistage model. *J. Phys. Chem. B* **107**, 10299-10311, doi:10.1021/jp027787v (2003).

22 Schicks, J. M. *et al.* Phase transitions in mixed gas hydrates: Experimental observations versus calculated data. *J. Phys. Chem. B* **110**, 11468-11474, doi:10.1021/jp0612580 (2006).

23 Schicks, J. M. & Ripmeester, J. A. The coexistence of two different methane hydrate phases under moderate pressure and temperature conditions: Kinetic versus thermodynamic products. *Angew. Chem.-Int. Edit.* **43**, 3310-3313, doi:10.1002/anie.200453898 (2004).

24 Clarke, M. A. & Bishnoi, P. R. Determination of the intrinsic kinetics of CO2 gas hydrate formation using in situ particle size analysis. *Chem. Eng. Sci.* **60**, 695-709, doi:10.1016/j.ces.2004.08.040 (2005).

25 Zhang, J. S., Lee, S. & Lee, J. W. Kinetics of methane hydrate formation from SDS solution. *Ind. Eng. Chem. Res.* **46**, 6353-6359, doi:10.1021/ie070627r (2007).

26 Kang, S. P., Seo, Y. & Jang, W. Kinetics of Methane and Carbon Dioxide Hydrate Formation in Silica Gel Pores. *Energy Fuels* **23**, 3711-3715, doi:10.1021/ef900256f (2009).

27 Takahashi, M. *et al.* Effect of shrinking microbubble on gas hydrate formation. *J. Phys. Chem. B* **107**, 2171-2173, doi:10.1021/jp02210z (2003).

28 Tajima, H., Yamasaki, A. & Kiyono, F. Continuous formation of CO2 hydrate via a kenics-type static mixer. *Energy Fuels* **18**, 1451-1456, doi:10.1021/ef034087w (2004).

29 Svandal, A., Kuznetsova, T. & Kvamme, B. Thermodynamic properties and phase transitions in the H2O/CO2/CH4 system. *Fluid Phase Equilib.* **246**, 177-184, doi:10.1016/j.fluid.2006.06.003 (2006).

30 Martin, A. & Peters, C. J. Thermodynamic Modeling of Promoted Structure II Clathrate Hydrates of Hydrogen. *J. Phys. Chem. B* **113**, 7548-7557, doi:10.1021/jp807367j (2009).

31 Klauda, J. B. & Sandler, S. I. Ab initio intermolecular potentials for gas hydrates and their predictions. *J. Phys. Chem. B* **106**, 5722-5732, doi:10.1021/jp0135914 (2002).

32 Rojas, Y. & Lou, X. Instrumental analysis of gas hydrates properties. *Asia-Pac. J. Chem. Eng.* **5**, 310-323, doi:10.1002/apj.293 (2010).

33 Mizuno, Y. & Hanafusa, N. STUDIES OF SURFACE-PROPERTIES OF ICE USING NUCLEAR-MAGNETIC-RESONANCE. *Journal De Physique* **48**, 511-517 (1987).

34 Takeya, S., Hondoh, T. & Uchida, T. in *Gas Hydrates: Challenges for the Future* Vol. 912 *Annals of the New York Academy of Sciences* (eds G. D. Holder & P. R. Bishnoi) 973-982 (New York Acad Sciences, 2000).

35 Uchida, T., Ebinuma, T., Kawabata, J. & Narita, H. Microscopic observations of formation processes of clathrate-hydrate films at an interface between water and carbon dioxide. *J. Cryst. Growth* **204**, 348-356, doi:10.1016/s0022-0248(99)00178-5 (1999).

36 Mondrakovski, I. L., Ratcliffe, C. I., McLaurin, G. E., Simard, B. & Ripmeester, J. A. Hydrate layers on ice particles and superheated ice: a H-1 NMR microimaging study. *J. Phys. Chem. A* **103**, 4969-4972 (1999).

37 Koh, C. A., Savidge, J. L. & Tang, C. C. Time-resolved in-situ experiments on the crystallization of natural gas hydrates. *J. Phys. Chem.* **100**, 6412-6414, doi:10.1021/jp960094s (1996).

Chapter 2 Single Step Desalination %Reduction through Gas Hydrate Formation Process

Abstract

Gas hydrate was formed to clean up artificial produced water, all experiments were performed under condition of pressure in the range of 450 to 800psi and temperature in the range of -1 to 1°C. The artificial produced water contains various dissolved ions, including Na^+, Ca^{2+}, Mg^{2+}, Cl^- and other ions, and the total dissolved solids (TDS) are in the range of 40,000 to 450. NaCl had the weakest inhibiting effect on gas hydrate formation and consumed the largest amount of CO_2. Higher NaCl concentration leads to longer induction time. The optimal incipient pressure of CO_2 consumption was obtained for both NaCl and $CaCl_2$. The $MgCl_2$ had the lowest desalination %Reduction while $CaCl_2$ obtained the highest by gas hydrate formation. The present study illustrated the optimal control condition during gas hydrate formation and CO_2 consumption; meanwhile it certificated the possibility of applying gas hydrate formation process in desalination.

2.1 Introduction

Gas hydrate belongs to a group of compound known as clathrate, in which water molecules are linked through hydrogen bonding and construct cavities (host lattice) that can enclose a large variety of molecules (guest). No chemical bonding exists between the host molecules and the enclosed guest molecules [4] . Clathrate formation causes a series of problems in oil and gas industry during the production, transportation processes. Large hydrated masses occurring in natural gas pipelines, for example, in Arctic regions and in the sea, can slow or completely obstruct flow. Also there has been a recent resurgence in developing methods to harvest the huge amount of methane present in natural gas hydrate, such as methane hydrate stored in the sediment in the deep ocean that could be regarded as a promising new energy supply, and natural gas stored in the earth crust. A recent estimate of methane amount trapped in hydrate is as much as 300 times that in conventional U. S. reserves [5] . Widely interests have been presented on the clathrate

hydrate properties, structure, and formation process during the last decades. Gas hydrates are thermodynamically stable under high pressure and near freezing temperature of pure water [6]. Although different gas has different thermodynamic stable pressure and temperature conditions, most of gas can form gas hydrate in specific conditions, including methane, carbon dioxide, hydrogen and some gas mixture.

Tsutomu Uchida et al. [8] worked on the kinetic and stability of CO_2 hydrate comparing to methane hydrate by using chromatography and Raman Spectroscopy. From their thermal calculation, they observed that methane molecules are preferentially crystallized in the early stages of hydrate formation when the initial methane concentration is much less than that of CO_2, and pure methane hydrate was first formed when existing together with CO_2. However in the reverse process, CO_2 is much easier to be released from CH_4-CO_2 mixture under the same condition.

Susan Circone et al. [9-11] searched on synthesis, composition and dissociation behavior of CO_2 hydrate in comparison with methane hydrate. They divided the dissociation behavior of CO_2 hydrate into two parts, one is when the temperature under 273 K, sI CO_2 hydrate dissociation is dominated by one characteristic: bulk of hydrate is released base on a time scale regardless of the pressure-temperature pathway the sample follows, which is in contrast with CH_4 that is highly temperature-pressure path dependent; another situation happens above 273 K, the observed dissociation behavior of CO_2 hydrate is consistent to that of CH_4 hydrate in that the internal temperature decreased below the H_2O melting point by following the pressure release until dissociation completed and then climb to the H_2O melting point.

Gang Li et al. studied on effect factors for CO_2 hydrate rapid formation in a water-spraying apparatus. They found that oscillating gas supply mode leads to larger gas consumption in the condition of continuous gas supply mode, due to large mass-transfer driving force. CO_2 has a larger solubility in gas hydrate formation, and thus larger volume of water in the vessel cause a large amount of gas consumption. In their spraying system, nozzle atomizing angle can be different and has various effects on the gas hydrate formation, they acquired that a larger nozzle atomizing angel cause shorter

induction time, explaining by the reason that making liquid water into spray micro fog drops or tiny particles can enhance the interface and contact areas significantly.

2.2 Experimental

Materials

Airgas carbon dioxide with a certificated purity of bone dry grade. Sodium Chloride of certificated ACS crystalline supplied by Fisher science Co.; Calcium Chloride supplied by Fisher Science Education with 4-20 mesh; and Magnesium Chloride supplied by Alfa Aesar Co. with purity of 99% were used.

EDTA (Ethylene diamineteraacetic acid disodium salt dehydrate) with a purity of 99+% supplied by Alfa Aesar Co. was used. Sodium Hydroxide with a purity of ≥98% supplied by Sigma-Aldrich Co. was used. Eriochrome Black T with pure indicator grade supplied by Acros Organic Co. and Patton & Reeders' (Calconcarboxylic acid) for complexometry were used as indicator in titration.

Analysis of Produced Water from Shale Gas Industry

Produced water (PWs) is generated during processes such as fossil fuel extraction, fossil fuel energy production, and industrial operations. In the continental US, major resources of PWs include conventional natural gas PWs, conventional oil PWs, coal-bed methane PWs, shale gas PWs and tight gas sands PWs [12] . Some produced water are released during or after fracturing of the source formation and gas recovery, such as coal-bed methane, shale gas and tight gas sands produced water [13] . Bethany Alley et al. [16] studied about chemical and physical characterization of produced water, they got the fact that significant difference were observed of calcium, potassium, magnesium, sodium iron, manganese, zinc and chloride concentrations between different kinds of produced water. In our sample data of shale gas onsite from NETL, we found that usually produced water includes bicarb, calcium, chloride, magnesium, potassium, potassium, sodium and many other organic components.

Table 2.1 Average concentrations of the various electrolytes present in produced water

Species	Ca^{2+}	Cl^-	Na^+	HCO_3^-
Avg. Conc. (mg/L)	4875	53621	24610	656
Species	Mg^{2+}	SO^{4-}	TDS	pH
Avg. Conc. (mg/L)	1028	1132	89254	7.14

Table 2.2 Major ion concentration in produced water from onsite data

Species	Ca^{2+}	Cl^-	Na^+	HCO_3^-	Mg^{2+}	SO_4^{2-}
Avg. Conc.(wt.%)	0.49	5.36	2.46	0.07	0.10	0.11

However, through the calculation and analysis, we acknowledged that major salt ions are chloride, magnesium, sodium and calcium and their corresponding concentration was shown in table 2.1 and table 2.2.

Experimental Apparatus

The main component of the apparatus consists of a stainless steel volume constant equilibrium vessel with a maximum volume of 100mL. The vessel is machined from a solid 316 stainless steel and equipped with a magnetic stirrer drive with a maximum rpm of 683.10. The maximum working pressure of the vessel is 3000psi, and the maximum working temperature is 350°C. The vessel is sealed with PTFE Gaskets as well as O-rings. The temperature inside is measured with a type J (iron constant) Omega thermocouple. The accuracy of the thermocouple measurement is believed to be ±0.10K. The pressure is measured by a 0-3000psi stainless steel Bourdon tube and 1/4" NPT male connections pressure gage from Parr Instrument Company. The coolant bath is Endocal RTE-series refrigerated circulating bath supplied by Neslab Co.

Experiment Procedures

Weighed 50g deionized H_2O and specific weight of salt on an electronic balance with a readability of ±0.1mg, put them all into a 200mL beaker, and kept magnetic stirring for 5min to prepare feed saline water, after the solution turning to clear and all solute

dissolved, finally discharged well stirred solution into the vessel. The uncertainty of the solution concentration was less than 0.2%. The computer-based data-acquisition system can automatically record real-time changes of pressure and temperature in the vessel every one second.

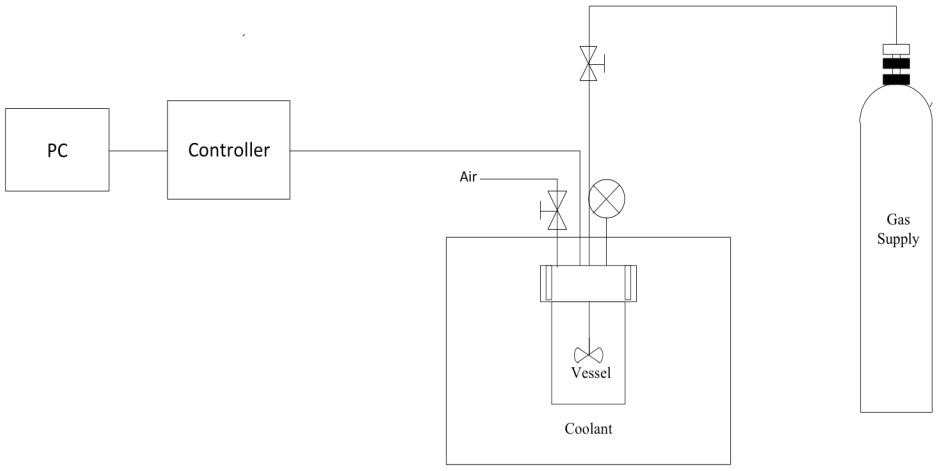

Figure 2.1 Schematic of the experimental apparatus in gas hydrate formation

The reaction vessel was rinsed three times with deionized water at the beginning. Sealed the reaction system and pumped CO_2 gas in a low pressure and room temperature in order to evacuate air or other gas in the gas system. Kept flowing CO_2 for around 15min under 25-35psi and room temperature to flush all the other gases with CO_2 in the vessel, then we stopped CO_2 gas flow and let the inner pressure decrease slowly and continuously to 0psi to make sure CO_2 was the only gas fulfilled the vessel. Pumped CO_2 gas once again into the vessel until the inside pressure reached 60psi, turned off the valve and put the vessel into coolant bath. Set the coolant bath temperature as 1°C, cooling down the vessel until the temperature inside stayed stable in 1°C for 3-4 hours. Started experiment by imputing CO_2, after the vessel was pressurized to an expected starting value; CO_2 was stopped and agitation was started at a speed of 683.10 rpm at the same time. As long as the reaction started, the system temperature was lowered, first frequently and then slowly, accompanying with the same trend of pressure to form hydrate. Each experiment acquired ending point of gas hydrate formation for 20min. Recorded the

temperature and pressure both at the starting and ending point, starting point was regarded as the point when we stopped imputing CO_2 and started agitation. If there was gas hydrate formed in the equilibrium vessel at the end of experiment run when temperature and pressure stayed in constant, then we counted this point right before the vessel was opened as ending point. Stopped agitation and opened the valve to discharge residual CO_2 inside the vessel until the inner pressure decrease to 0psi. Opened the vessel in room temperature when two parts were obtained, CO_2 hydrate in solid phase and dirty water in liquid phase. We moved gas hydrate and dirty water parts into two beakers separately, tested the concentration of each part with correct ion-test techniques. The schematic of the experimental apparatus for gas hydrate formation is shown in **Figure 2.1**.

Measurement of Na^+ Ion Concentration

CON 510 Bench Conductivity/TDS Conductivity Meter was used to test sodium ion concentration. Calibrated the ion meter with standard solution before measurement. Prepared NaCl solutions with weight concentrations range from 0.01 to 0.1wt.%, recorded corresponding conductivity every 0.01wt.%, and plotted the relationship between concentrations and conductivity. We get linearly relation between concentration and conductivity through following equation:

$$Concentration = 5\times10^{-5}Conductivity - 0.0034 \quad (2.1)$$

in the equation, concentration unit is wt.%, and conductivity unit is μS/cm. From the above equation, we can calculate NaCl concentration according to conductivity.

Measurement of Ca^{2+} Ion Concentration

EDTA titration was used to detect Ca concentration. Prepared a 0.005mol L^{-1} EDTA solution and 8mol L^{-1} NaOH solution. EDTA (ethylenediaminetetraacetic acid) forms a complex with calcium ions. Used Patton-Reeder indicator triturate as indicator of end point.

For the titration, the indicator is added to the sample solution containing the calcium ions and forms the pink/red calcium ion-indicator complex (Ca-PR). This solution is then titrated with EDTA. The endpoint occurs when the solution turns blue, indicating that the

Ca-PR complex has been completely replaced by the calcium ion-EDTA complex and the PR indicator reverts to its blue color.

The reaction is:

$$Ca - PR + EDTA^{4-} \rightarrow PR + [Ca - EDTA]^{2-} \quad (2.2)$$

Pipetted a 10mL of the unknown solution into a 250ml conical flask. Added 40mL distilled water and 4mL sodium hydroxide solution of 8mol L^{-1}, and allowed solution to stand for about 5min with occasional swirling. Added the indicator after you have given this precipitate a chance to form. Added 0.1g of Patton-Reeder indicator and swirled the solution to dissolve the indicator. Titrated the sample with the EDTA solution. Recorded volume use of EDTA solution and calculated with following equation to get Ca^{2+} concentration:

$$Ca^{2+}\ Concentration\ of\ unknown\ solution = \frac{V(EDTA)\times c(EDTA)}{V(sample)} \quad (2.3)$$

unit of Ca^{2+} concentration is mol L^{-1}.

Measurement of Mg^{2+} Ion Concentration

EDTA titration method was used to detect Mg^{2+} concentration. The reaction of Mg^{2+} with EDTA (Ethylenediaminetetraacetic acid) may be expressed as:

$$Mg^{2+} + H_2Y^{2-} \rightarrow MgY^{2-} + 2H^+ \quad (2.4)$$

Chose unknown solution, pipetted 3ml of unknown solution into a conical flask, added approximately 10ml of buffer and 50ml deionized water into the flask; added 4 drops of Eriochrome Black T indicator (aq.) and we got a light, wine-red color. Titrated solution with standardized EDTA solution to a clear blue color. Recorded volume of EDTA used in titration. Use following equation to calculate the concentration of unknown solution:

$$Mg^{2+}\text{Concentration of unknown solution} = \frac{\text{V(EDTA)}\times\text{c(EDTA)}}{\text{V(sample)}} \quad (2.5)$$

unit of Mg^{2+} concentration we get from above equation is mol L^{-1}.

Estimation of Carbon Dioxide Consumption

Gas consumption was calculated in the base of ideal gas law modification with compressibility factor, pressure and temperature in both starting point and ending point when gas hydrate formed, which was also used by Hyun Ju Lee. et al. [17]. Following equation was used to calculate the moles of CO_2 consumed.

$$\Delta n = \left(\frac{PV}{zRT}\right)_0 - \left(\frac{PV}{zRT}\right)_t \quad (2.6)$$

where compressibility factor, z, is calculated by CO_2 critical point and present point with temperature and pressure; P and T are from read of reactor; while V is approximately equal to volume of reactor minus volume of water in the reactor.

Calculation of %Reduction of Salts

We defined desalination %Reduction with following equation:

$$\%Reduction = \frac{c_0 - c_{product}}{c_0} \times 100\% \quad (2.7)$$

in which c_0 is feed water concentration, and $c_{product}$ is concentration in final gas hydrate solid product.

2.3 Results and Discussion

Effect of Feed Water Concentration on the CO_2 Consumption

Table 2.3 Experimental data of %Reduction of salts with different TDS.

Salts	Concentration	One-stage% reduction	Salts	Concentration	One-stage% reduction
NaCl	6.00	16.29	$CaCl_2$	1.50	47.87
	10.00	22.04		2.50	40.40
	18.00	19.37		3.00	35.34
	20.00	9.91		3.50	16.58
	0.80	4.43		4.50	10.03
	1.08	8.19		5.00	12.57
	2.00	3.55		0.0140	8.77
$MgCl_2$	0.13	7.13		0.0516	23.93
	0.50	6.00		0.4880	23.73
	1.00	1.15			

Table 2.4 Initial concentration, pressure and temperature of three salts in different concentrations and their corresponding CO_2 consumption

Salt	Initial Concentration (wt%)	P(psi)	T (°C)	CO_2 Consumption (mol)	Salt	Initial Concentration (wt%)	P(psi)	T (°C)	CO_2 Consumption (mol)
NaCl	1.08	637	4.50	0.0600	$CaCl_2$	1.50	802	7.30	0.0385
	1.08	649	7.70	0.0428		2.00	801	8.30	0.0385
	1.08	649	7.70	0.0397		2.50	802	8.60	0.0373
	1.08	650	7.70	0.0429		3.00	796	10.30	0.0346
	1.08	650	10.40	0.0449		3.50	703	7.30	0.0256
	1.08	645	8.00	0.0423		4.00	699	7.00	0.0260
	1.08	654	7.60	0.0432		4.50	702	6.90	0.0322
	2.00	653	6.60	0.0384		5.00	697	6.80	0.0240
	2.00	636	5.40	0.0388		5.50	700	7.00	0.0263
	2.00	651	8.00	0.0411		0.49	489	5.80	0.0235
	2.00	656	8.00	0.0394		0.49	497	5.60	0.0211
	0.80	648	8.20	0.0376		0.10	502	5.00	0.0218
	0.80	655	7.10	0.0528		0.05	493	6.00	0.0228
	0.80	650	6.90	0.0352		0.03	490	4.80	0.0224
	6.00	706	6.00	0.0273		0.01	499	6.00	0.0225
	8.00	544	2.30	0.0162		0.02	589	5.50	0.0284
	10.00	800	3.70	0.0430		0.01	515	3.40	0.0288
	10.00	701	6.00	0.0282		0.04	501	5.00	0.0218
	15.00	801	8.20	0.0428		0.03	497	1.00	0.0209
	20.00	801	8.30	0.0444		0.49	504	4.70	0.0208
	1.08	454	3.20	0.0394		0.05	494	5.90	0.0227
	1.08	511	2.50	0.0477	$MgCl_2$	0.13	486	6.50	0.0240
	1.08	539	3.20	0.0180		0.50	493	5.20	0.0229
	1.08	605	5.70	0.0609		1.00	477	6.00	0.0254
	1.08	654	5.30	0.0660					
	1.08	702	7.80	0.0612					

Experimental data are recorded and listed in table 2.3 and table 2.4.

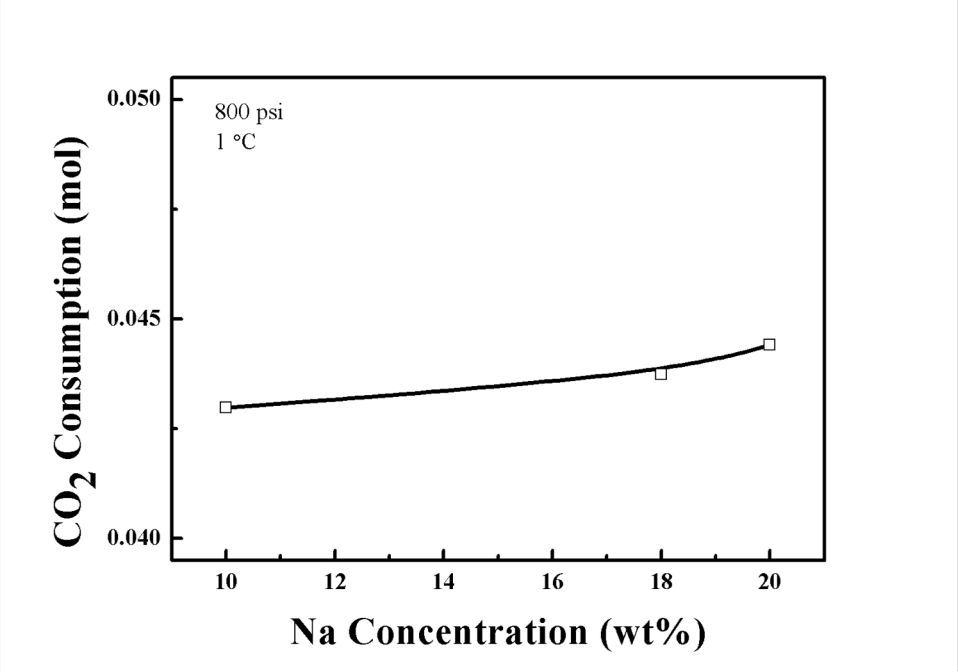

Figure 2.2 Effect of Na^+ concentration in feed water on the CO_2 consumption, with initial pressure as 800psi and temperature as 1°C.

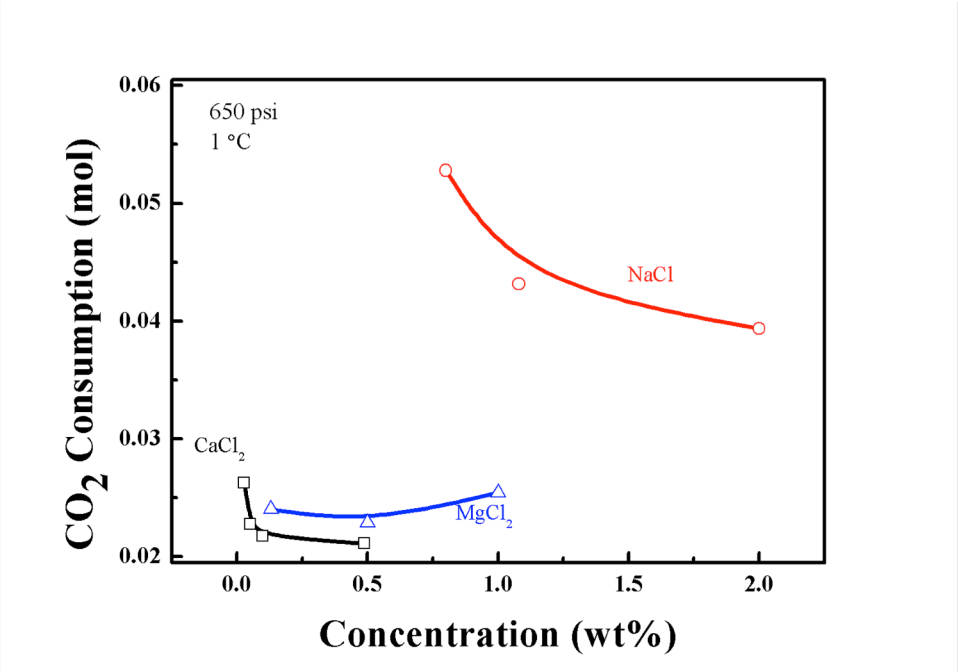

Figure 2.3 Effect of different ion kind and concentration in feed water on the CO_2 consumption, with initial pressure as 800psi and temperature as 1°C.

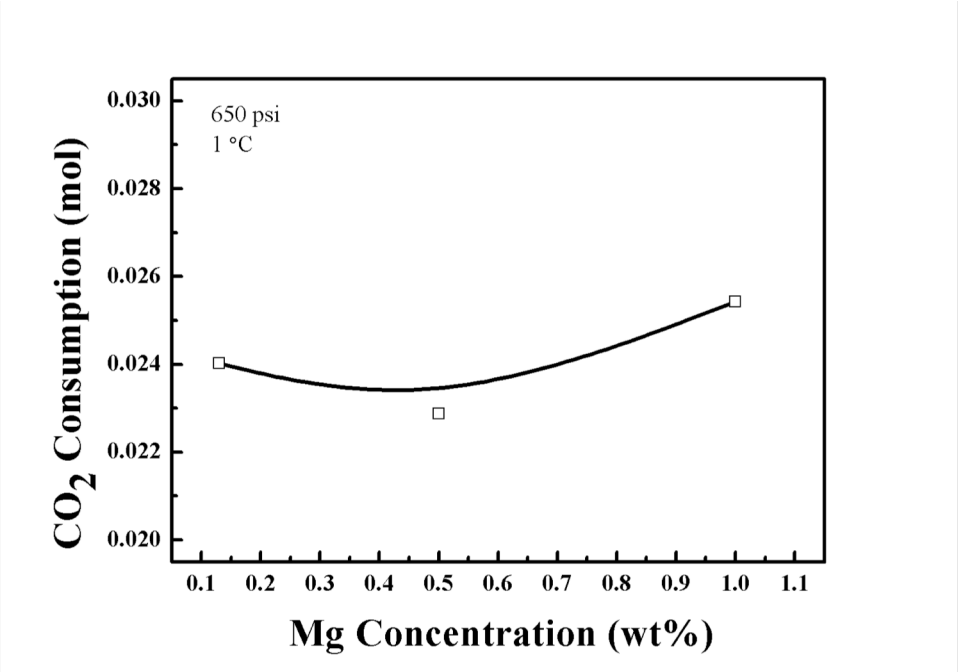

Figure 2.4 Effect of Mg^{2+} concentration in feed water on the CO_2 consumption, with initial pressure as 650psi and temperature as 1°C.

For NaCl solution, in high concentration range from 10 to 20wt.% as shown in Figure 2.2, with initial condition of 800psi and 1°C, CO_2 consumption increased from 0.0428 to 0.0444moles as concentration increased. This implies CO_2 solubility increases in gas hydrate formed in higher concentration feed water.

Figure 2.3 shows CO2 consumption decreases from 0.0528 to 0.0394moles as concentration increases in low concentration range, which is in agreement with Pankaij D. Dholabhai 1 research that they saw clear inhibiting effect of NaCl with concentration between 3 to 5wt.%. Higher concentration tends to consume more CO2 in average, indicating stronger inhibiting effect on gas hydrate formation and CO2 consumption. Under the gas hydrate formation conditions of 650psi and 1°C, the mole consumption of both MgCl2 and CaCl2 are much lower than that of NaCl solution, indicating CaCl2 and MgCl2 own stronger inhibiting effect in gas hydrate formation.

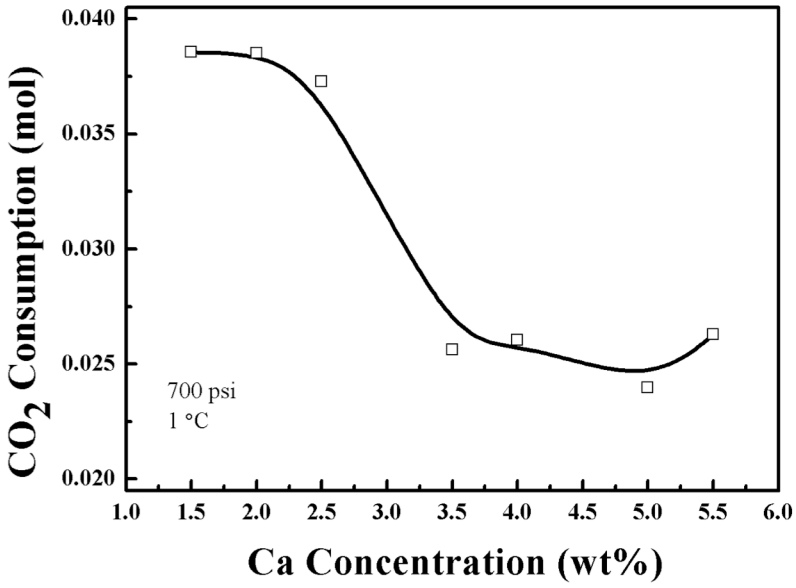

Figure 2.5 Effect of Ca^{2+} concentration in feed water on the CO_2 consumption, with initial pressure as 700psi and temperature as 1°C.

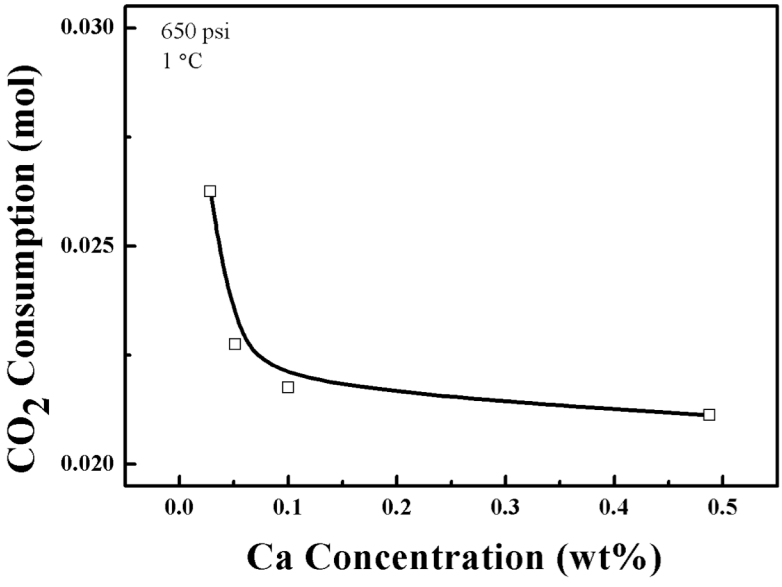

Figure 2.6 Effect of Ca^{2+} concentration in feed water on the CO_2 consumption, with initial pressure as 800psi and temperature as 1°C.

As shown in Figure 2.4, 0.024moles CO2 is captured in 0.13wt.% MgCl2, the consumption amount goes first down and then up to 0.0254 mole as the concentration rise

to 1.0wt.%. The first part is in agreement with Seong-Pil Kang et al. 1 theory about the MgCl2 inhibiting effects on CO2 hydrate formation and thus encapsulate less gas. We try to explain the second part for the reason that CO2 solubility in concentration higher than 0.5wt.% cannot be ignored any more.

Figure 2.5 shows the CO_2 capture ability in concentration range of 1.5 to 5.5wt.% $CaCl_2$, concentration point is chosen every 0.5 wt.% under same initial condition of 700psi and 1°C. In the first region of 1.5 to 2.5wt.%, $CaCl_2$ concentration growth leads to less CO_2 consumed smoothly, in the second region of 2.5 to 3.5wt.%, the CO_2 consumption decreases rapidly; in the third region, CO_2 consumption stayed almost the same. In the first two regions, the inhibiting effect of $CaCl_2$ is observed obviously.

In low concentration range shown in Figure 2.6, addition of $CaCl_2$ leads to CO_2 consumption reduction. Overall, it seems like that $CaCl_2$ owns a stronger inhibiting effect on gas consumption in low concentration than that in high concentration range, which is opposite to general acknowledgement. We explain this phenomenon by different pressure manipulated.

Effect of Initial Pressure on the CO_2 Consumption

We carried out CO_2 hydrate formation under different incipient pressure varied from 450 to 700psi by controlling temperature in a specific value of 1°C. 1.08wt.% NaCl and 0.015wt.% $CaCl_2$ were chosen as supply water separately, with pressure point gathered every 50psi, and corresponding CO_2 consumption were calculated.

Figure 2.7 shows that when we increase pressure from 450 to 650psi, gas consumption rise gradually and reaches the largest mole consumption of 0.066 moles at 650psi, but if pressure is further improved to 700psi, a decrease of consumed CO_2 is observed. It implies that an optimal pressure on gas consumption is obtained and as higher pressure leads to a larger driving force, and larger driving force promotes CO_2 sequestration.

In 0.015wt.% $CaCl_2$ solution as shown in **Figure 2.8**, an optimal pressure of 720psi on gas consumption is noted, which is in consistent with NaCl. Overall, larger driving force

causes more CO_2 incorporated in clathrate structure, but an optimal pressure appeared with the most CO_2 captured, and pressure too high inhibits CO_2 encapsulated.

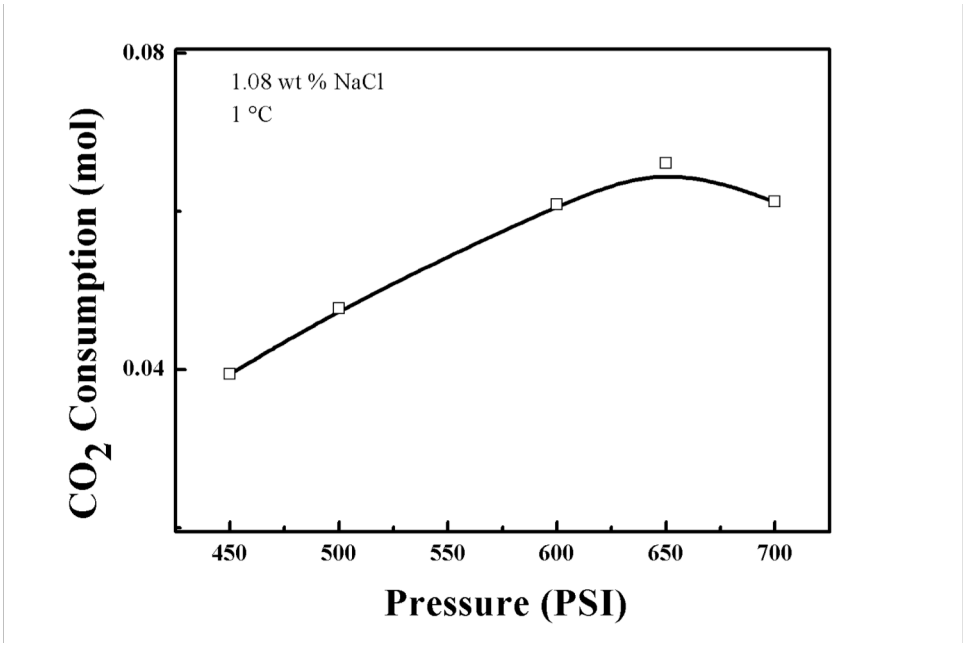

Figure 2.7 Effect of initial pressure on the CO_2 consumption, with feed water as 1.08wt.% NaCl and initial temperature as 1°C.

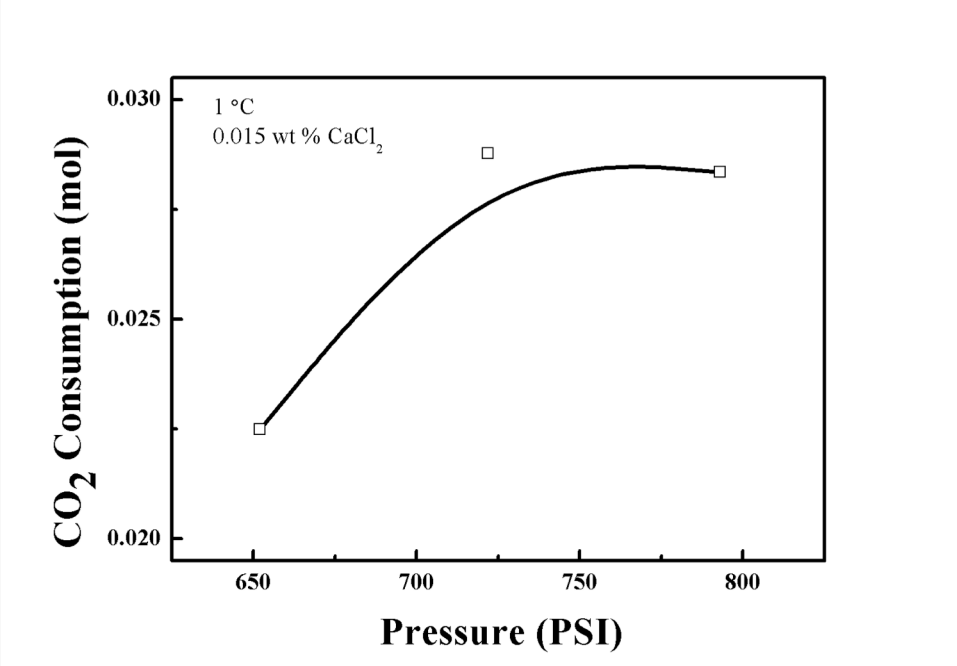

Figure 2.8 Effect of initial pressure on the CO_2 consumption, with feed water as 0.015wt.% $CaCl_2$ and initial temperature as 1°C.

Effect of Feed Water Concentration on the Induction Time

Artificial brine solutions in various TDS were prepared and their corresponding curves of pressure-reaction time are plotted. In curve of pressure-reaction time, a spike indicating the starting point of gas hydrate formation is observed and time period from beginning to the spike is defined as induction time. According to Rajnish Kumar et al. [2] visual observation of hydrate growth， extensive hydrate formation and crystal agglomeration results in accumulation of crystal as a stagnant layer at the gas/water interface, which prevents more gas from contacting with water.

In **Figure 2.9**, pressure-reaction time curves of NaCl in concentration from 10 to 18wt.% are presented. Induction time increase from 3 to 15min as concentration improves from 10 to 18wt.%, which confirms what we obtained earlier that higher NaCl concentration owns stronger inhibiting effect on gas hydrate formation. In general, the induction time is shorter as the driving force increases. [3] From above-mentioned, increment of concentration leads to weaker driving force, and longer time for nucleation in high concentration range.

Induction time in low NaCl concentration range are shown in **Figure 2.10**, indicating that under incipient formation condition of 650 psi and 1 °C, 1.08wt.% results in the shortest induction time of 1min, while 2.0wt.% has the longest. We are able to figure out that there is an optimal concentration of 1.08wt.% on induction time. Overall, brine concentration increment leads to stronger inhibiting effect though it is not obvious in low concentration range.

For $MgCl_2$, it is can be seen in **Figure 2.11** that the shortest induction time is obtained in 1wt.%, while the longest time happened in 0.5wt.%. In this way, it is reasonable to conclude that either increasing or decreasing concentration from 0.5wt.%, can we start gas hydrate formation in a shorter time and inhibiting effect of Mg concentration is not significant in this region either.

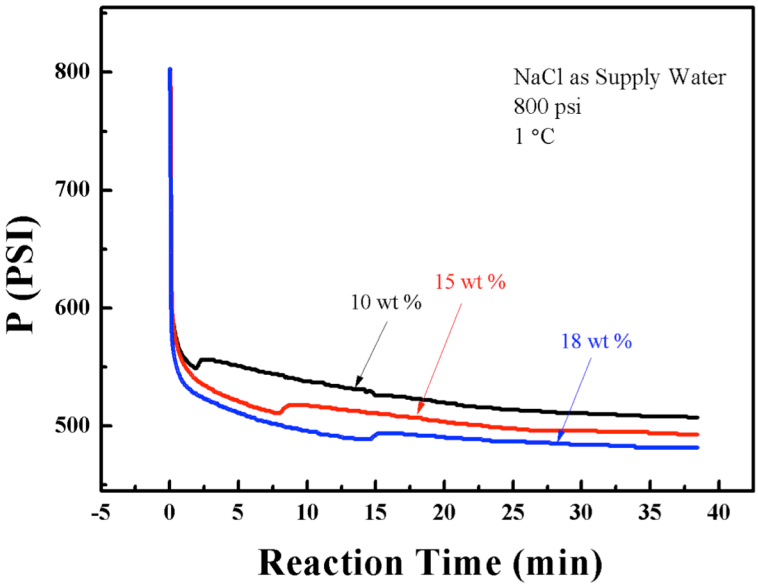

Figure 2.9 Effect of Na^+ concentration in feed water on the induction time, with initial pressure as 800psi and temperature as 1°C.

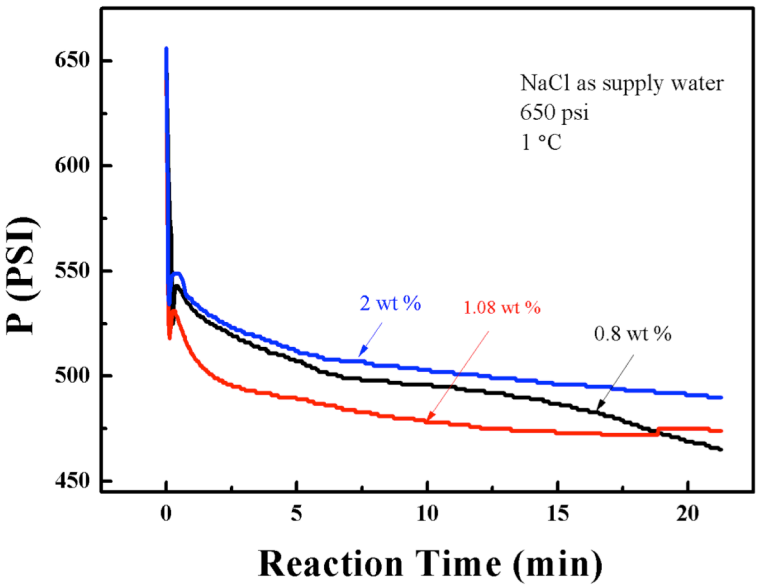

Figure 2.10 Effect of Na^+ concentration in feed water on the induction time, with initial pressure as 650psi and temperature as 1°C.

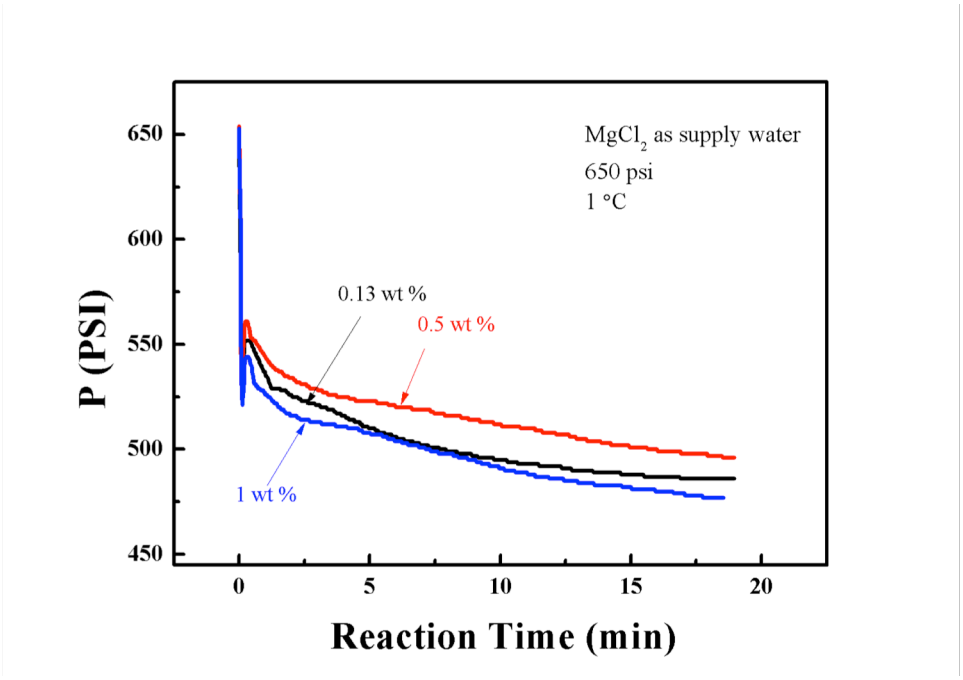

Figure 2.11 Effect of Mg^{2+} concentration in feed water on the induction time, with initial pressure as 650psi and temperature as1°C.

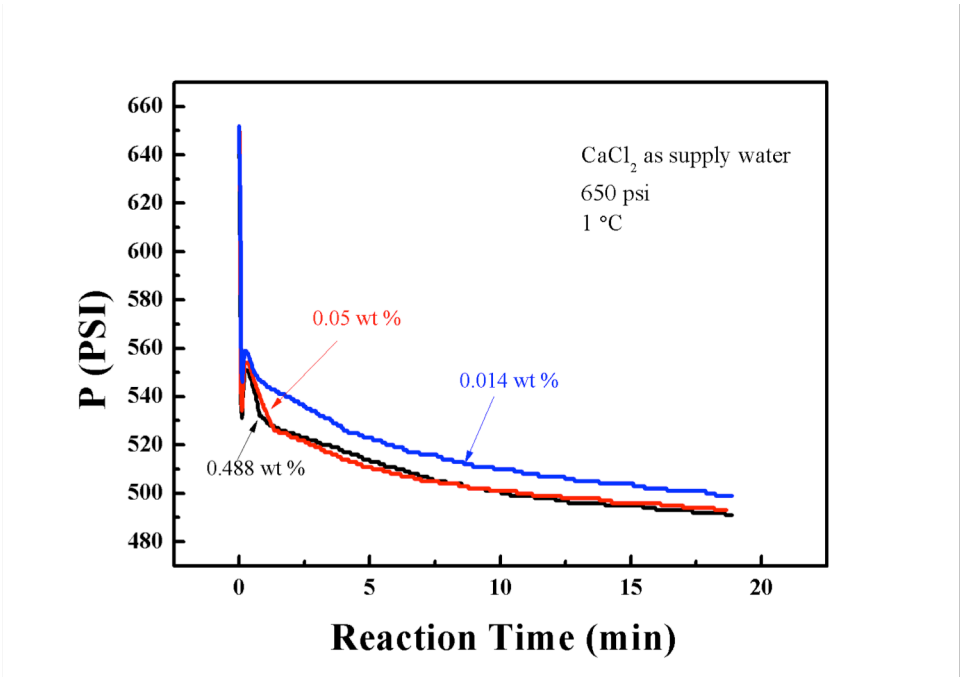

Figure 2.12 Effect of initial pressure on the induction time, with feed water as $CaCl_2$, pressure as 800psi and temperature as 1°C.

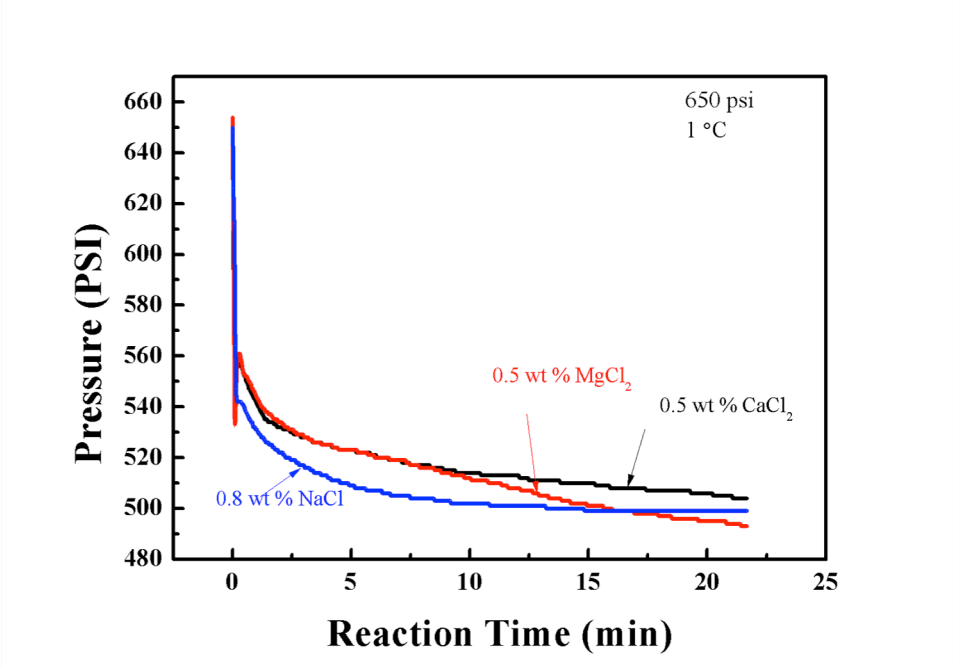

Figure 2.13 Effect comparison of different ions on the induction time, with pressure as 650 psi and temperature as 1 °C.

No obvious impact of Ca concentration on induction time is observed in **Figure 2.12**, more tests need to be operated if we wanted to explore the correct relation between concentration and induction time in $CaCl_2$.

We produced gas hydrate formation with different brine and results are plotted in **Figure 2.13**. It indicates that NaCl obtains the shortest induction time while 0.5 $CaCl_2$ and $MgCl_2$ has almost the same induction time. No obvious difference of induction time between brine water is observed from **Figure 2.13**.

Effect of Initial Pressure on the Single-Stage Desalination %Reduction

All experimental data were collected and shown in table 3 and plotted in **Figure 2.14**, it indicates that %Reduction improved from 11.62 to 38.44% and decreases after as the increase of initial pressure from 450 to 650psi. We figured out an optimal formation pressure of 650psi.

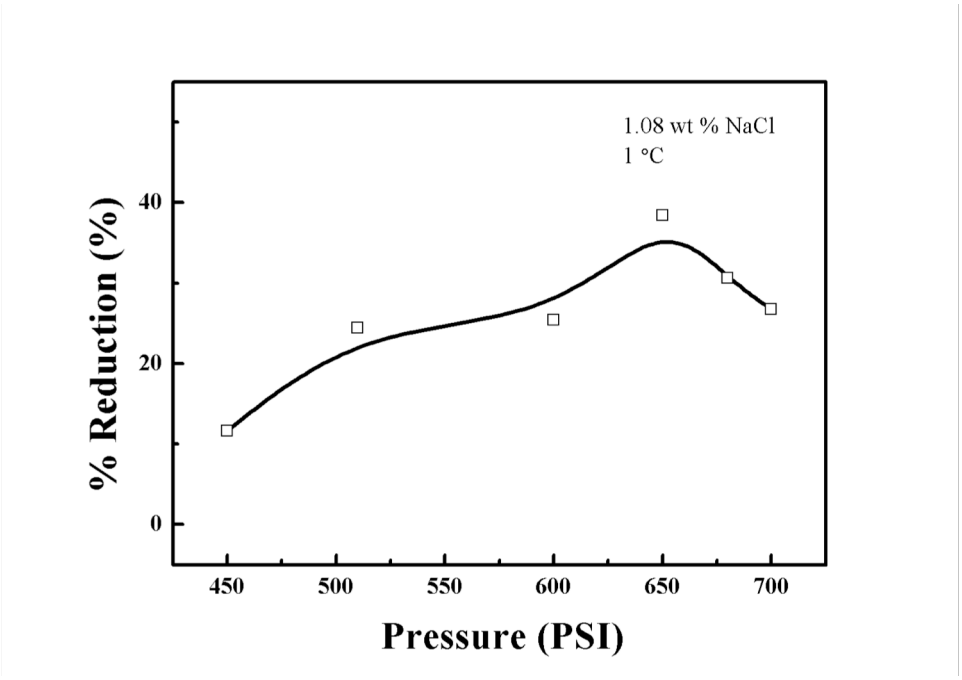

Figure 2.14 Effect of initial pressure on the %Reduction, with feed water as 1.08wt.% NaCl and initial temperature as 1°C.

Effect of Feed Water Concentration on the Single-Stage Desalination %Reduction

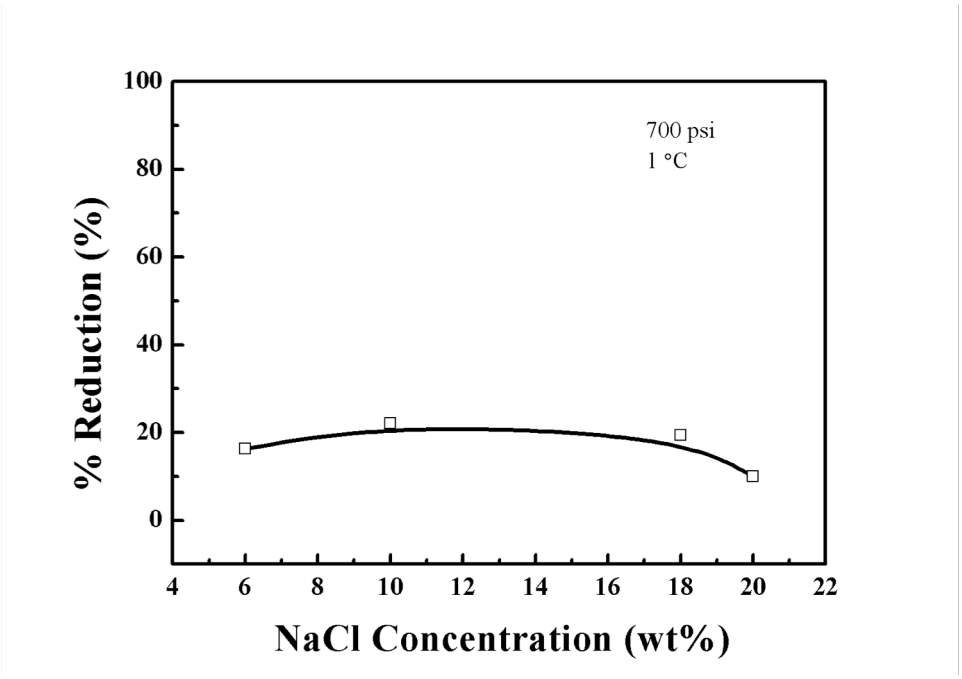

Figure 2.15 Effect of Na^+ concentration in feed water on the %Reduction, with pressure as 700psi and temperature as 1°C.

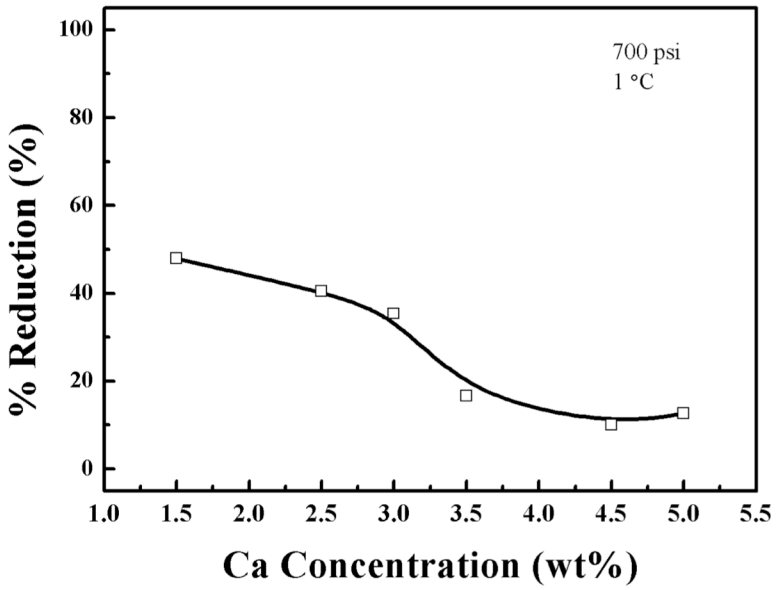

Figure 2.15 Effect of Ca^{2+} concentration in feed water on the %Reduction, with initial pressure as 700psi and temperature as 1°C.

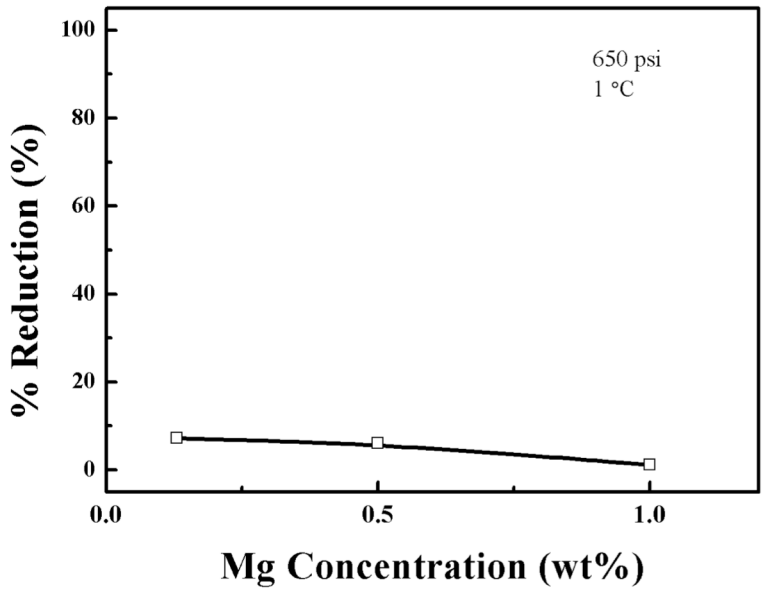

Figure 2.16 Effect of Mg^{2+} concentration in feed water on the %Reduction, with initial pressure as 650psi and temperature as 1°C.

In higher concentration region (>1.0 wt.%), %Reduction of NaCl in various concentrations were presented in **Figure 2.**.It was observed the optimal concentration of 10 wt.%. Overall, the average %Reduction was as low as 20 %.

Experimental data of $CaCl_2$ were shown in **Figure 2.15**, it could be seen that increase of Ca concentration from 1.5 to 4.5wt.% brings %Reduction of $CaCl_2$ from 47.87 down to 10.03%, and %Reduction stays almost the same in concentration higher than 4.5wt.%. Overall, we found that higher concentration doesn't result in lower %Reduction and vice versa for both salts and higher %Reduction of $CaCl_2$ than that of NaCl.

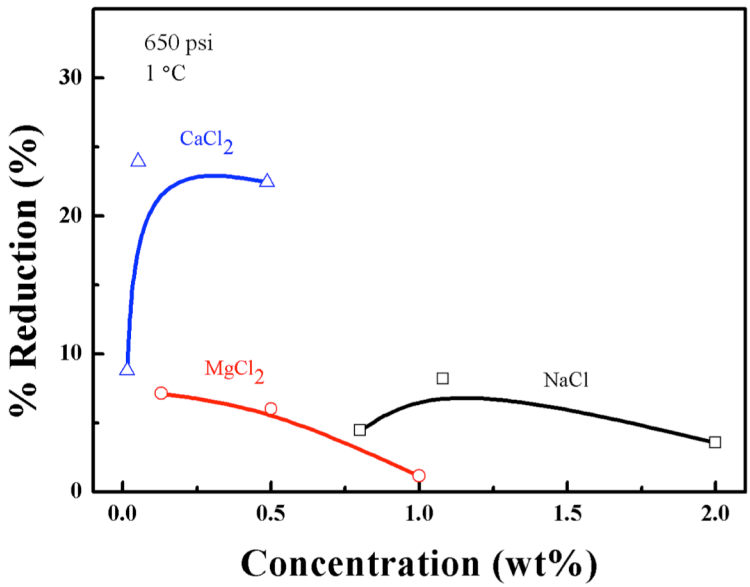

Figure 2.17 Effect comparison of different TDS in feed water on the %Reduction, with initial pressure as 650psi and temperature as 1°C.

In lower concentration region (<1.0 wt.%), all of experiments performed under condition of 650 psi and 1 °C. Figure 2.16 implies that increment of Mg concentration leads to %Reduction fell from 7.13 down to 1.15%.

In **Figure 2.17** we compared three brine feed water concentration effects on %Reduction; we figured out that an optimal concentration of $CaCl_2$ happened on 0.05wt.% while NaCl appeared on 1.08wt.%. We found that decreasing concentration doesn't cause better %Reduction for NaCl and $CaCl_2$ solution, however, for $MgCl_2$

solution, decreasing concentration improves %Reduction. Among three brine waters, $CaCl_2$ achieved the highest average %Reduction of 18.38 %, while $MgCl_2$ had the lowest %Reduction. Overall, it is reasonable to assume that gas hydrate formation desalination method works better on higher concentration salt water.

2.4 Conclusions

Gas consumption and %Reduction of salt were calculated, associated induction time were recorded and compared. Artificial produced water with different TDS was chosen as feed water under controlled pressure and temperature. In higher concentration range, increasing NaCl concentration leads to the CO_2 larger consumption; while an optimal concentration on gas consumption is obtained in $CaCl_2$. In lower concentration range, lower concentration causes more CO_2 consumed for both NaCl and $CaCl_2$.

When the TDS variation was big enough for NaCl, higher TDS leads to longer induction time and weaker driving force. But no apparent effects of brine feed water TDS on induction time when TDS varied in a small range.

Lower concentration helps to remove more salt component in artificial produced water. In comparison of three brines, $CaCl_2$ achieves the highest average %Reduction, while $MgCl_2$ has the least. Gas hydrate formation works better on higher TDS range for both $CaCl_2$ and NaCl.

2.5 References

1 Englezos, P. CLATHRATE HYDRATES. *Ind. Eng. Chem. Res.* **32**, 1251-1274, doi:10.1021/ie00019a001 (1993).

2 Sloan, E. D. *Clathrate Hydrate of Natural Gases*. (CRC Press, 1998).

3 J. H. van der Waals, J. C. P. <CLATHRATE SOLUTIONS.pdf>. doi:10.1002/9780470143483.ch1.

4 Uchida, T. *et al.* Kinetics and stability of CH4-CO2 mixed gas hydrates during formation and long-term storage. *ChemPhysChem* **6**, 646-654, doi:10.1002/cphc.200400364 (2005).

5 Giavarini, C., Maccioni, F., Politi, M. & Santarelli, M. L. CO2 hydrate: Formation and dissociation compared to methane hydrate. *Energy Fuels* **21**, 3284-3291, doi:10.1021/ef070080t (2007).

6 Li, G., Liu, D. P., Xie, Y. M. & Xiao, Y. Study on Effect Factors for CO(2) Hydrate Rapid Formation in a Water-Spraying Apparatus. *Energy Fuels* **24**, 4590-4597, doi:10.1021/ef100417y (2010).

7 Veil, A., Puder, M.G., Elcock, D., Redweik, R.J.,Jr.,. A White Paprt Describing Produced Water from Production of Crude Oil, Natural Gas, and Coal Bed Methane. . (United States Department of Energy and National Energy Technology Laboratory, 2004).
8 Petroleum: Fossil Fuel Production. US Energy Information Administration: Independent Statistics and Analysis., (United States Department of Energy, 2010).
9 Jones, F. O. & Owens, W. W. A Laboratory Study Of Low-Permeability Gas SandS. *J. Pet. Technol.* **32**, 1631-1640 (1980).
10 Jones, A. H., Bell, G.J., Schraufngel, R.A.,. A review of the physical and mechanical properties of coal with implications for coalbed methane well completion and production: coalbed merhane, San Juan Basin. . (Rockey Mountain Association of Geologists, 1988).
11 Curtis, J. B. Fractured shale-gas systems. *AAPG Bull.* **86**, 1921-1938 (2002).
12 Alley, B., Beebe, A., Rodgers, J. & Castle, J. W. Chemical and physical characterization of produced waters from conventional and unconventional fossil fuel resources. *Chemosphere* **85**, 74-82, doi:10.1016/j.chemosphere.2011.05.043 (2011).
13 Lee, H. J. *et al.* Gas hydrate formation process for pre-combustion capture of carbon dioxide. *Energy* **35**, 2729-2733, doi:10.1016/j.energy.2009.05.026 (2010).
14 Dholabhai, P. D., Kalogerakis, N. & Bishnoi, P. R. Equilibrium Conditions For Carbon-Dioxide Hydrate Formation In Aqueous-Electrolyte Solutions. *J. Chem. Eng. Data* **38**, 650-654, doi:10.1021/je00012a045 (1993).
15 Kang, S. P., Chun, M. K. & Lee, H. Phase equilibria of methane and carbon dioxide hydrates in the aqueous MgCl2 solutions. *Fluid Phase Equilib.* **147**, 229-238, doi:10.1016/s0378-3812(98)00233-7 (1998).
16 Kumar, R., Linga, P., Ripmeester, J. A. & Englezos, P. Two-Stage Clathrate Hydrate/Membrane Process for Precombustion Capture of Carbon Dioxide and Hydrogen. *J. Environ. Eng.-ASCE* **135**, 411-417, doi:10.1061/(asce)ee.1943-7870.0000002 (2009).
17 Linga, P., Kumar, R. N. & Englezos, P. Gas hydrate formation from hydrogen/carbon dioxide and nitrogen/carbon dioxide gas mixtures. *Chem. Eng. Sci.* **62**, 4268-4276, doi:10.1016/j.ces.2007.04.033 (2007).

Chapter 3 Dewatering of Gas Hydrate Formed from Artificial Produced Water

Abstract

The results obtained in this study showed that over 99% of dissolved NaCl and $MgCl_2$ can be removed from artificial saline water in a process involving a single-stage hydrate formation step, followed by a single-step dewatering. The hydrate crystals were cut into small pieces and placed in vials and centrifuged. The results show that the %Reduction (percentage of the concentration decrease) of NaCl increases with centrifugation time and rotational speed (rpm) after the centrifugation. In filtration, artificial produced water containing 0.8 to 2.0wt.% NaCl was used as feed water. The resulting hydrate crystals were crushed using a mortar and pestle and subjected to vacuum filtration. As shown, the values of %Reduction of NaCl were substantially higher than obtained using the centrifuge. The %Reduction increased with increasing filtration time as anticipated. Also, the process is effective over a wide range of salinity, which is an advantage over reverse osmosis. After reducing the particle size further by grinding, %Reduction reached 90%, indicating that the finer the particle size, the higher the extent of cleaning.

3.1 Introduction

Gas hydrates are ice-like crystalline compounds that are formed by the combination of water with gas molecules under suitable pressure and temperature conditions. The water molecules through hydrogen bonding are capable of forming a three-dimensional lattice structure containing cavities. These cavities can be occupied by molecules of gases and volatile liquids whose molecular diameter is smaller than that of the cavity. By the consumption of gas or liquid molecules, the structure, by itself thermodynamically unstable, is stabilized. Each cavity structure may contain one guest molecule.

Based on the fact that gas hydrate is capable to form a solid substance consisting of clean water and gas molecules only, the possibility of using gas hydrate for water desalination has been investigated during the last decades [4,5] and is actively being developed at industrial scale at present. The process of gas hydrate formation and

decomposition are exothermal and endothermic respectively, which can cause their mutual inhibition during phase changes. Meanwhile, we can achieve energy consumption enhancement by optimizing the exothermal and endothermic processes by utilizing heat produced in hydrate formation process on the melting of hydrate in further stage of the desalination. The objective of modern desalination industry field requires producing a large amount of clean water in a short period and with the minimum energy consumptions. In this way, optimizations of the gas hydrate formation and further stages in the desalination process are urgently needed [6] .

CO_2 hydrate forms at very high pressure but the low cost of CO_2, the ease of stripping it from solution, its low corrosive impact on the apparatus, lack of toxicity and flammability [7] put it in a promising place in desalination industry.

M. D. Jager and E. D. Sloan [8] worked on the effect of pressure on methane hydrate in sodium chloride solutions and pure water. Djurdjica Corak et al. [6] explored the effect of subcooling and amount of formation of cyclopentane hydrate in brine and obtained the desalination efficiency through the gas hydrate formation process. The removal of NaCl varied from 89 to 73% with the best value obtained under temperature condition of 5.6 K and 3.6 K in atmosphere pressure. Larger amount of gas hydrate formed under 3.6 K series and the residual salinity is likely to be strongly related to the procedure for separating the solid hydrate phase from residual water. From the relationship between adhesion forces and temperature concluded by A.G. Speight [9] , they also obtained that the attractive force between hydrate particles was stronger and thus hydrate crystal adhered each other in a more tight framework formed at 3.6 K than the one at 5.6 K, and that means more brine will be entrapped between the crystals; extraction procedure like centrifuge was performed to remove this part of brine.

Zadjia Atik et al. [10] found that gas hydrate dissociation pressure for pure methane in different electrolyte solutions. They compared the effect of $MgCl_2$ and $CaCl_2$ on the methane hydrate formation, $MgCl_2$ solution had a stronger ability to lower water activity and thus a higher prevention capability, and it also causes a larger freezing point depression than $CaCl_2$ does. P. R. Bishnoi and P. D. Dholabhai [11] tried to acquire the equilibrium conditions of propane hydrate in aqueous electrolyte solutions. They used

two methods, one is keeping temperature in constant and increased the system pressure, while another was setting both temperature and pressure as constant and then decreases temperature, to determine the gas hydrate equilibrium conditions.

A. M. Aliev et al. [12] developed a mathematical model of seawater desalination through gas hydrate method, they calculated the optimal feed rate of gas hydrate formation apparatus and total height of working part if their apparatus applied in industry field.

3.2 Experimental

Materials

Airgas carbon dioxide with a certificated purity of bone dry grade. Sodium Chloride of certificated ACS crystalline supplied by Fisher science Co.; Calcium Chloride supplied by Fisher Science Education with 4-20 mesh; and Magnesium Chloride supplied by Alfa Aesar Co. with purity of 99% were used.

EDTA (Ethylene diamineteraacetic acid disodium salt dehydrate) with a purity of 99+% supplied by Alfa Aesar Co. was used. Sodium Hydroxide with a purity of ≥98% supplied by Sigma-Aldrich Co. was used. Eriochrome Black T with pure indicator grade supplied by Acros Organic Co. and Patton & Reeders' (Calconcarboxylic acid) for complexometry was used as indicator in titration.

Analysis of Produced Water from Shale Gas Industry

Produced water (PWs) is generated during processes such as fossil fuel extraction, fossil fuel energy production, and industrial operations. [13] In the continental US, major resources of PWs include conventional natural gas PWs, conventional oil PWs, coal-bed methane PWs, shale gas PWs and tight gas sands PWs [14] . Some produced water are released during or after fracturing of the source formation and gas recovery, such as coal-bed methane, shale gas and tight gas sands produced water [15-17] . Bethany Alley et al. [18] studied about chemical and physical characterization of produced water, they got the fact that significant difference were observed of calcium, potassium, magnesium, sodium iron, manganese, zinc and chloride concentrations between different kinds of produced water. In our sample data of shale gas onsite from NETL, we found that usually produced water

includes bicarb, calcium, chloride, magnesium, potassium, potassium, sodium and many other organic components.

Table 3.1 Average concentrations of the various electrolytes present in produced water

Species	Ca^{2+}	Cl^-	Na^+	HCO_3^-
Avg. Conc. (mg/L)	4875	53621	24610	656
Species	Mg^{2+}	SO^{4-}	TDS	pH
Avg. Conc. (mg/L)	1028	1132	89254	7.14

Table 3.2 Major ion concentration in produced water from onsite data

Species	Ca^{2+}	Cl^-	Na^+	HCO_3^-	Mg^{2+}	SO_4^{2-}
Avg. Conc.(wt.%)	0.49	5.36	2.46	0.07	0.10	0.11

However, through the calculation and analysis, we acknowledged that major salt ions are chloride, magnesium, sodium and calcium and their corresponding concentration was shown in table 3.1 and table 3.2.

Measurement of Na^+ Ion Concentration

CON 510 Bench Conductivity/TDS Conductivity Meter was used to test sodium ion concentration. Calibrated the ion meter with standard solution before measurement. Prepared NaCl solutions with concentrations range from 0.01 to 0.1wt.%, recorded corresponding conductivity every 0.01wt.%, and plotted the relationship between concentrations and conductivity. We get linearly relation between concentration and conductivity through following equation:

$$Concentration = 5\times10^{-5}Conductivity - 0.0034 \quad (3.1)$$

in the equation, concentration unit is wt.%, and conductivity unit is μS/cm. From the above equation, we can calculate NaCl concentration according to conductivity.

Measurement of Ca^{2+} Ion Concentration

EDTA titration was used to detect Ca concentration. Prepared a 0.005mol L^{-1} EDTA solution and 8mol L^{-1} NaOH solution. EDTA (ethylenediaminetetraacetic acid) forms a complex with calcium ions. Used Patton-Reeder indicator triturate as indicator of end point.

For the titration, the indicator is added to the sample solution containing the calcium ions and forms the pink/red calcium ion-indicator complex (Ca-PR). This solution is then titrated with EDTA. The endpoint occurs when the solution turns blue, indicating that the Ca-PR complex has been completely replaced by the calcium ion-EDTA complex and the PR indicator reverts to its blue color.

The reaction is:

$$Ca - PR + EDTA^{4-} \rightarrow PR + [Ca - EDTA]^{2-} \quad (3.2)$$

Pipetted a 10mL of the unknown solution into a 250ml conical flask. Added 40mL distilled water and 4mL sodium hydroxide solution of 8mol L^{-1}, and allowed solution to stand for about 5min with occasional swirling. Add the indicator after you have given this precipitate a chance to form. Added 0.1g of Patton-Reeder indicator and swirled the solution to dissolve the indicator. Titrated the sample with the EDTA solution. Recorded volume use of EDTA solution and calculated with following equation to get Ca^{2+} concentration:

$$Ca^{2+}\ Concentration\ of\ unknown\ solution = \frac{V(EDTA)\times c(EDTA)}{V(sample)} \quad (3.3)$$

unit of Ca^{2+} concentration is mol L^{-1}.

Measurement of Mg^{2+} Ion Concentration

EDTA titration method was used to detect Mg^{2+} concentration. The reaction of Mg^{2+} with EDTA (Ethylenediaminetetraacetic acid) may be expressed as:

$$Mg^{2+} + H_2Y^{2-} \rightarrow MgY^{2-} + 2H^+ \quad (3.4)$$

Chose unknown solution, pipetted 3ml of unknown solution into a conical flask, added approximately 10ml of buffer and 50ml deionized water into the flask; added 4 drops of Eriochrome Black T indicator (aq.) and we got a light, wine-red color. Titrated solution with standardized EDTA solution to a clear blue color. Recorded EDTA volume use in titration. Use following equation to calculate the concentration of unknown solution:

$$\mathrm{Mg^{2+}Concentration\ of\ unknown\ solution} = \frac{\mathrm{V(EDTA)\times c(EDTA)}}{\mathrm{V(sample)}} \quad (3.5)$$

unit of Mg^{2+} concentration we get from above equation is mol L^{-1}.

Measurement of Total Mg^{2+} and Ca^{2+} Ions Concentration

Using EDTA titration and a blue dye called Eriochrome Black T (ErioT) is used as the indicator. This blue dye forms a complex with the calcium and magnesium ions, changing color from blue to pink in the process. The dye–metal ion complex is less stable than the EDTA–metal ion complex. For the titration, the sample solution containing the calcium and magnesium ions is reacted with an excess of EDTA. The indicator is added and remains blue as all the Ca^{2+} and Mg^{2+} ions present are complexes with the EDTA.

A back titration is carried out using a solution of magnesium chloride. This forms a complex with the excess EDTA molecules until the end-point, when all the excess EDTA has been a complex. The remaining magnesium ions of the magnesium chloride solution then start to complex with ErioT indicator, immediately changing its color from blue to pink.

The main reactions are:

$$Ca^{2+} + EDTA^{4-} \rightarrow [Ca - EDTA]^{2-} \quad (3.6)$$

$$Mg^{2+} + EDTA^{4-} \rightarrow [Mg - EDTA]^{2-} \quad (3.7)$$

$$ErioT + Mg^{2+} \rightarrow ErioT - Mg \quad (3.8)$$

Note: ErioT is blue and ErioT-Mg is pink.

We can use following equation to calculate the final total magnesium and calcium ion concentration:

$$Total\ (c_{Mg} + c_{Ca}) = \frac{V(EDTA)\times c(EDTA) - V(MgCl_2)\times c(MgCl_2)}{V(sample)} \quad (3.9)$$

Unit of total concentration we got from the above equation was mol L^{-1}.

Experimental Procedure

Weighed 50g deionized H_2O and specific weight of salt on an electronic balance with a readability of ±0.1mg, put them all into a 200mL beaker, and kept magnetic stirring for 5min to prepare feed saline water, after the solution turning to clear and all solute dissolved, finally discharged well stirred solution into the vessel. The uncertainty of the solution concentration was less than 0.2%. The computer-based data-acquisition system can automatically record real-time changes of pressure and temperature in the vessel every one second.

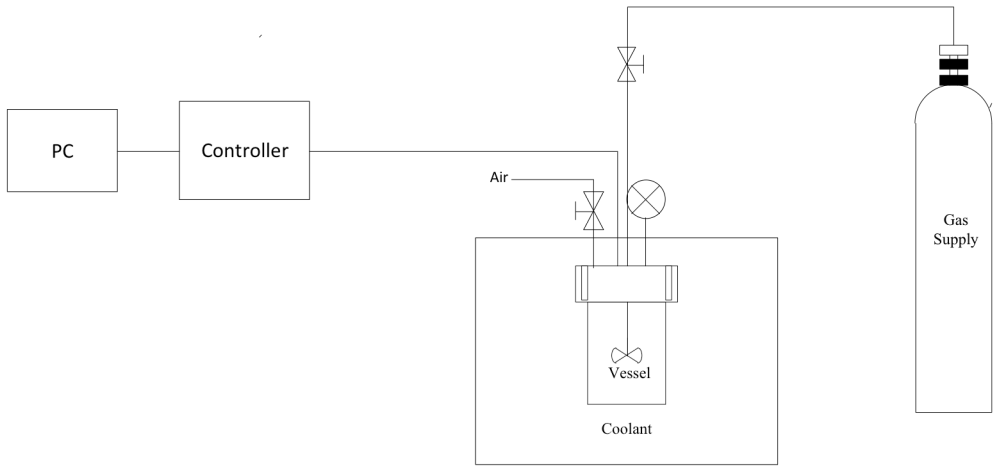

Figure 3.1 Schematic of the experimental apparatus in gas hydrate formation

The reaction vessel was rinsed three times with deionized water at the beginning. Sealed the reaction system and pumped CO_2 gas in a low pressure and room temperature in order to evacuate air or other gas in the gas system. Kept flowing CO_2 for around 15min under 25-35psi and room temperature to flush all the other gases with CO_2 in the

vessel, then we stopped CO_2 gas flow and let the inner pressure decrease slowly and continuously to 0psi to make sure CO_2 was the only gas fulfilled the vessel. Pumped CO_2 gas once again into the vessel until the inside pressure reached 60psi, turned off the valve and put the vessel into coolant bath. Set the coolant bath temperature as 1°C, cooling down the vessel until the temperature inside stayed stable in 1°C for 3-4 hours. Started experiment by imputing CO_2, after the vessel was pressurized to an expected starting value; CO_2 was stopped and agitation was started at a speed of 683.10 rpm at the same time. As long as the reaction started, the system temperature was lowered, first frequently and then slowly, accompanying with the same trend of pressure to form hydrate. Each experiment acquired ending point of gas hydrate formation for 20 min. Recorded the temperature and pressure both at the starting and ending point, starting point was regarded as the point when we stopped imputing CO_2 and started agitation. If there was gas hydrate formed in the equilibrium vessel at the end of experiment run when temperature and pressure stayed in constant, then we counted this point right before the vessel was opened as ending point. Stopped agitation and opened the valve to discharge residual CO_2 inside the vessel until the inner pressure decrease to 0psi. Opened the vessel in room temperature when two parts were obtained, CO_2 hydrate in solid phase and dirty water in liquid phase. We moved gas hydrate and dirty water parts into two beakers separately, tested the concentration of each part with correct ion-test techniques.

The experimental apparatus for gas hydrate formation was shown in Figure 3.1. Two parts were obtained after gas hydrate formation: CO_2 hydrate in solid phase and dirty water in liquid phase. In principle, CO_2 hydrate is formed with pure water, thereby excluding dissolved impurities. However, the residual water containing high-salinity brines are trapped in between the hydrate crystals. Therefore, it is necessary to go through a solid-liquid separation (or dewatering) process before melting the hydrate crystals to obtain pure water. We chose two different separation methods.

1) Centrifuge
2) Filtration with vacuum pump

Centrifugation Dewatering Procedure

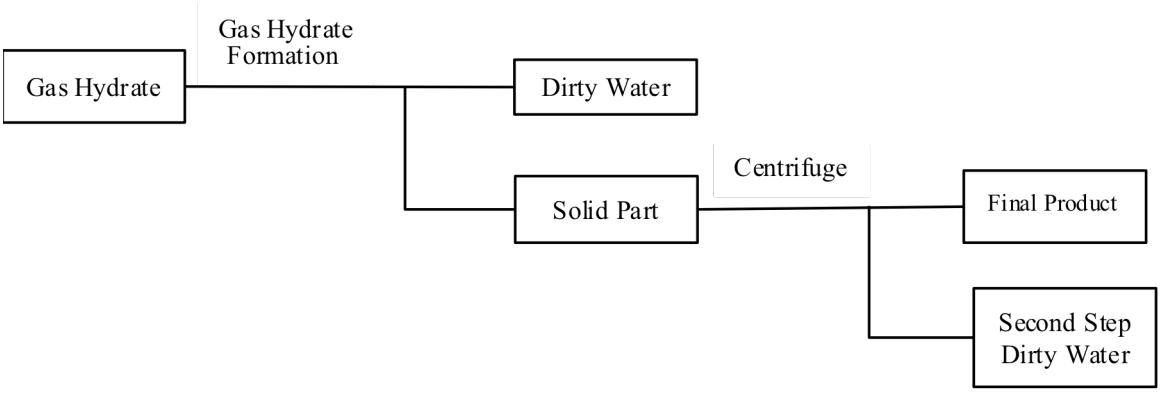

Figure 3.2 Flow sheet of desalination process involving gas hydrate formation and centrifugation.

A Centrifuge (IEC CENTRA CL2) from Thermo ELECTRON COPORATION In. with the maximum rpm of 8500 and the minimum of 3900 was used in the centrifuge process. We used electrolyte with selected TDS as feed water to form gas hydrate in a series of experiments. Two parts were obtained after gas hydrate formation, one is named as dirty water in liquid phase and the other part is gas hydrate product in solid phase. Separated gas hydrate from dirty water and put both parts into beakers. We crushed solid gas hydrate into finer particles with spatula, so that we were able to put small particles into 6 tubes separately, guaranteed each tube had equal amount of gas hydrate in order to keep the balance of centrifuge machine. Put 6 tubes into centrifuge machine, set different centrifuge times while keeping rpm in a specific value, then set different rpms and keep centrifuge time as constant to study effects of time and rpm on desalination reduction separately. After centrifugation, we obtained two components in the tubes, melting gas hydrate in liquid phase and solid gas hydrate, poured melting part into one beaker and left solid gas hydrate in the tube until it melted completely in the room temperature, then poured it into the third beaker. Finally we got three parts: dirty water from first stage, final gas hydrate product and second stage dirty water from centrifuge process. Tested and recorded specific ion concentration of three parts separately, then calculated the mass balance of the whole process to improve the degree of confidence. The saline component of final hydrate product was measured and compared to supply water salinity to define

the desalination %Reduction of two-stage separation. The desalination with gas hydrate formation- centrifugation process is presented in **Figure 3.2**.

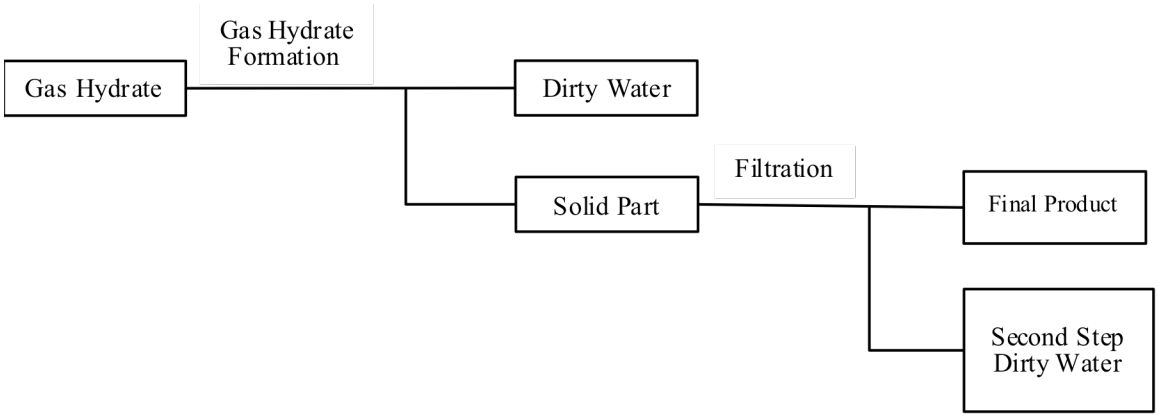

Figure 3.3 Flow sheet of desalination process involving gas hydrate formation and filtration.

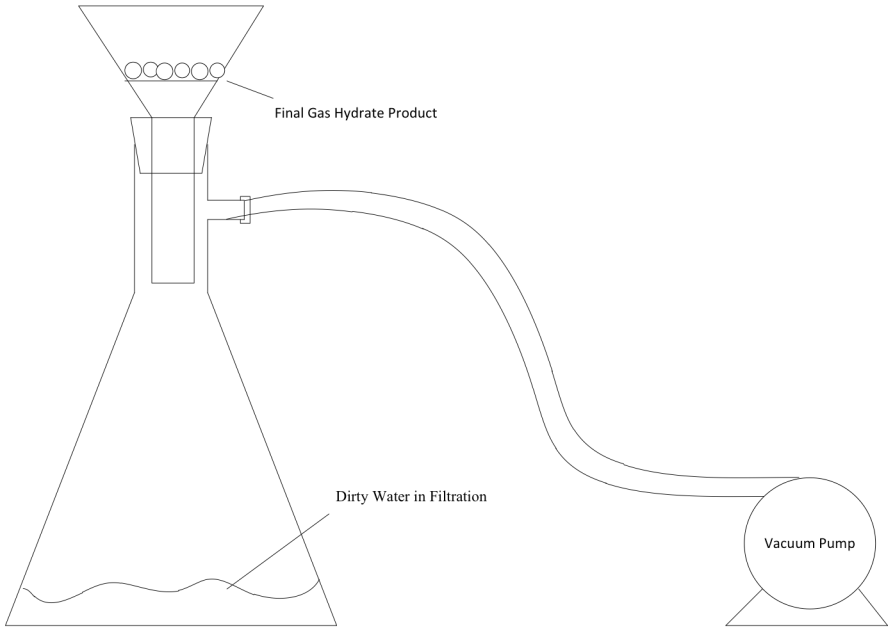

Figure 3.4 Schematic of the experimental apparatus in filtration

Filtration Dewatering Procedure

A vacuum pump (G 608 ex Mode) from GAST was used to produce vacuum in the filtration process. Before filtration, all the filtrating set-up including conical flask, funnel

were cleaned with deionized water twice to keep the clean of equipment. We used electrolyte in selected concentration as feed water in a consequence of experiment. Two parts were obtained after gas hydrate formation: one part is called dirty water in liquid phase and another part was gas hydrate product in solid phase. Separated gas hydrate product from dirty water and treated solid gas hydrate in two ways: 1）Crushed solid hydrate with spatula into small pieces; 2）Ground solid hydrate with mortar and pestle into finer particles. Then we discharged liquid and solid gas hydrate mixture into a funnel covered by filter paper on the top. Started the vacuum pump and recorded filtration time with stopwatch. After the filtration, gas hydrate was separated into two parts, one is final product in solid phase which left on the top of filter paper, and another part is dirty water went through filter paper in filtration. Measured and recorded ion concentration and volume of three parts in order to improve the degree of confidence through mass balance calculation. The saline concentration of final hydrate product was measured and compared to supply water salinity to define the desalination %Reduction of two-stage separation. The flow sheet of desalination with gas hydrate formation-filtration process is presented in

Figure 3.3 and experimental set-up of filtration was shown in **Figure 3.4**.

3.3 Results and Discussion

Table 3.3 Data obtained in centrifuge, including the centrifuge time, rpm, single-stage %Reduction, two-stage %Reduction and volume yield

Salt Name	Concentration	Centrifuge Time	RPM	single-stage % reduction	Two-stage % reduction	Whole Process Yield
NaCl	1.08	90	5000	30.36	68.09	5.60
	1.08	120	5000	22.67	74.16	4.80
	1.08	30	5000	21.94	26.09	20.00
	1.08	120	3000	24.15	61.25	10.80
	1.08	60	3000	24.42	34.10	22.00
	1.08	90	3000	23.34	46.52	19.00
	1.08	30	3000	8.94	17.40	30.00
	1.08	120	2000	16.28	42.26	10.00
	1.08	120	2000	26.68	54.15	12.50

Table 3.4 Data obtained in filtration, including the filtration time, single-stage %Reduction, and two-stage %Reduction, wash water addition and volume yield.

Salty Name	Concentration	Filtration Time	One-stage % Redcution	Two-stage % Reduction	wash water	Yield (%)
NaCl	1.08	120	21.05	25.53	no	60.00
	1.08	180	30.60	88.64	no	23.00
	1.08	240	13.70	56.73	no	46.00
	1.08	300	16.37	52.92	no	50.00
	1.08	360	7.30	98.43	no	10.00
	1.08	360	5.79	82.31	no	27.00
	1.08	420	7.55	93.58	no	26.00
	1.08	300	5.69	97.14	no	16.00
	2.00	300	18.05	52.34	no	38.00
	2.00	240	20.73	43.60	no	42.00
	0.80	240	14.16	62.38	no	36.00
	0.80	300	15.07	78.07	no	40.00
	1.08	360	8.19	90.92	10 s	
	0.80	360	4.43	95.84	10 s	
	2.00	360	3.55	94.55	10 s	
	2.00	420	6.10	97.45	10 s	
$CaCl_2$	0.4880	360	27.07	59.96	no	48.00
	0.4880	360	23.73	71.58	no	42.00
	0.1000	360	14.65	57.94	no	42.00
	0.0500	360	19.65	64.13	no	36.00
	0.0284	360	22.44	39.51	no	40.00
	0.0142	360	27.04	60.63	no	30.00
	0.0154	360	24.81	60.08	no	44.00
	0.0144	360	25.26	44.41	no	46.00
	0.0392	360	27.90	58.63	no	43.00
	0.0284	240	31.37	88.00	no	18.60
	0.4864	240	22.45	89.08	no	14.00
	0.0516	240	23.93	91.34	no	17.60
	0.0140	240	8.77	86.69	no	3.40
$MgCl_2$	0.13	360	7.13	99.19	no	18.00
	0.50	360	6.00	99.71	no	14.00
	1.00	360	1.15	98.84	no	2.80

All the result has been collected and shown in table 3.3 and 3.4.

Dewatering by Centrifugation

At the beginning, we need to clarify the definition of desalination %Reduction in the process with following equation:

$$Desalinaton\ \%reduction = \frac{c_1 - c_{product}}{c_1} \times 100\ \% \quad (3.10)$$

in which c_1 is the centrifuge feed water concentration; $c_{product}$ is the final solid hydrate product concentration.

Djurdjica Corak et al [6] obtained 87 to 67% NaCl removal of 3.5wt.% NaCl solution under 3.6K and atmosphere pressure, while under 5.6K and atmosphere pressure from 89 to 73% NaCl was removed after involving centrifuge process.

We used 1.08wt.% NaCl solution as feed water and in order to guarantee the consistence and reproducibility of centrifuge samples, consistent formation condition of 650psi and 1°C were controlled, each experiment was carried out twice. After centrifugation, the water released from the small crystals was decanted off, and the remaining crystals were allowed to dissociate.

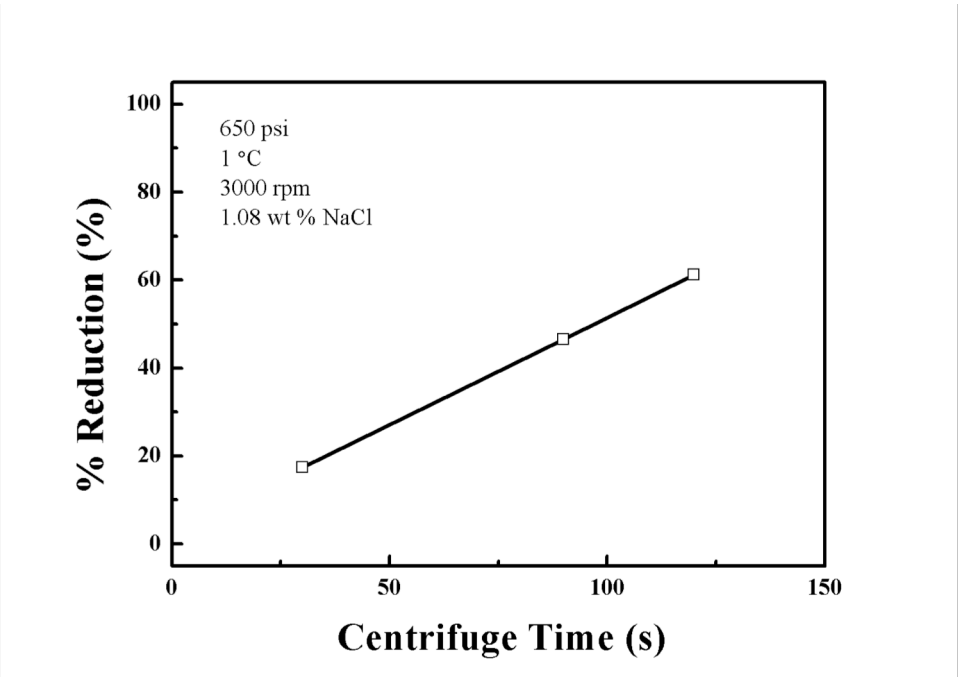

Figure 3.5 Effect of centrifuge time on %Reduction, with initial pressure as 650 psi and temperature as 1°C; 1.08wt.% NaCl is feed water and rpm is fixed as 3000

.

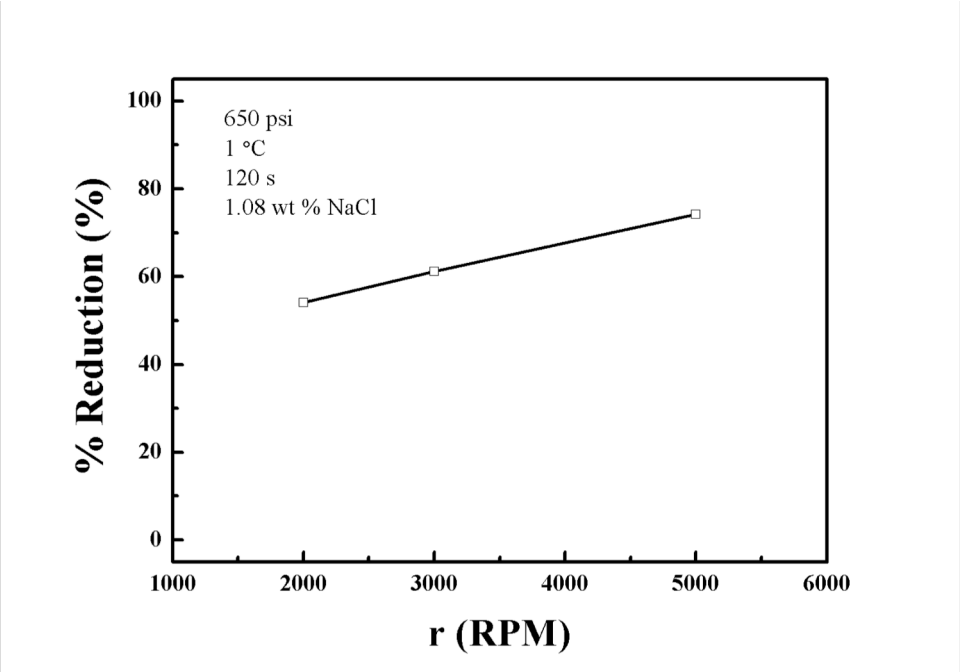

Figure 3.6 Effect of rpm on desalination %Reduction, with initial pressure as 650psi and temperature as 1°C; 1.08wt.% NaCl is feed water and centrifuge time is 120s.

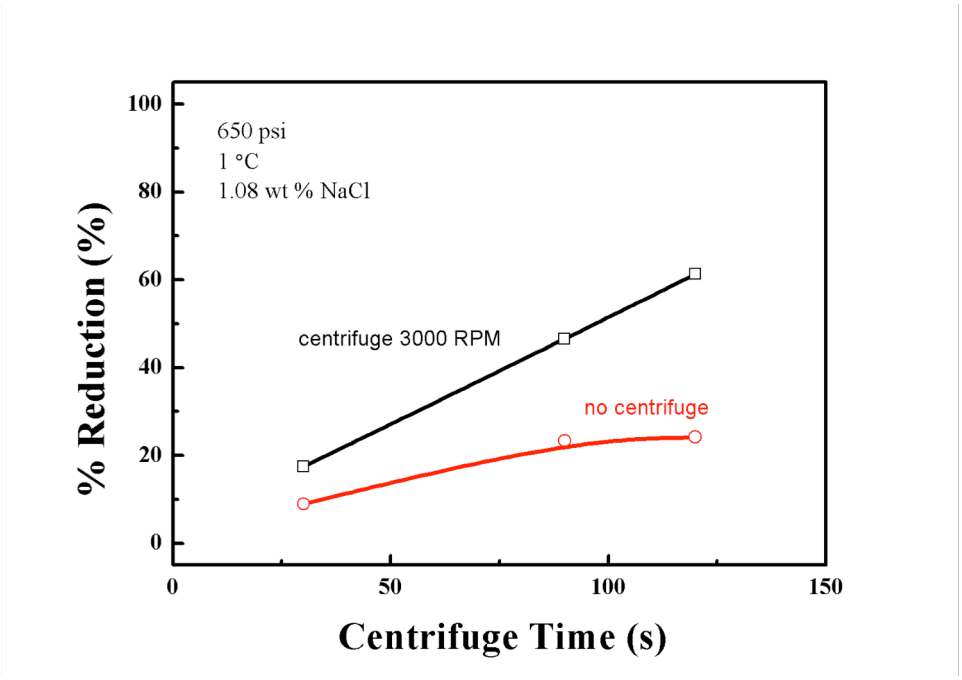

Figure 3.7 Comparison of %Reduction before and after centrifugation, with initial pressure as 650psi and temperature as 1°C, 1.08wt.% NaCl as feed water.

Figure 3.5 and **Figure 3.6** show results about effects of centrifuge time and rpm on %Reduction; it is obviously that the %Reduction of NaCl increased with centrifugation time and rotational speed (rpm). We obtained that the %reduction relates to centrifuge time linearly by following equation:

$$\%Reduction = 0.487\times Centrifuge\ time + 2.763 \tag{3.11}$$

and %Reduction relates linearly with centrifuge rpm by following equation:

$$\%Reduction = 0.00664\times Centrifuge\ RPM + 41.05 \tag{3.12}$$

The increase in efficiency with increasing rpm was due to the increase in the G-force that removes the entrapped water. Note, however, that the hydrate crystals still contained entrapped water, which may be attributed to two reasons. First, the entrapped water removed by centrifugation was removed by decantation rather than filtration; therefore, part of the residual water still remained with the crystals. Centrifugal filtration would have given better results. Second, the particle size of the broken hydrate crystals was too large. Crushing the crystals to finer sizes would have given better results. In **Figure 3.7**, gas hydrate formation centrifuge process does enhance the desalination %reduction.

But the volume yield goes into the opposite direction as %reduction. We define volume yield by following equation:

$$Volume\ Yield = \frac{V\ (clean\ water\ product)}{V\ (supply\ water)}\times 100\ \% \tag{3.13}$$

In **Figure 3.8** and

Figure 3.9, when centrifuge time and rpm increase, the volume yield is brought down sharply. This is explained that longer centrifuge time leads to gas hydrate exposed to room temperature for longer period and more contacts with room temperature tube, thus higher fractions of gas hydrate melts in the room temperature.

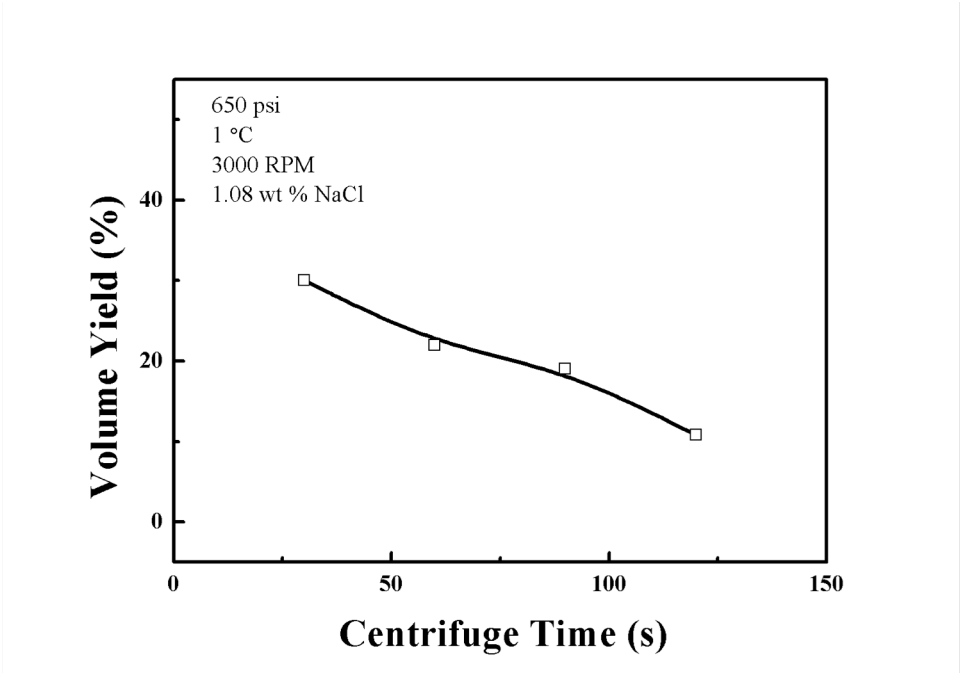

Figure 3.8 Effect of centrifuge time on volume yield, with initial pressure as 650psi and temperature as 1°C; 1.08wt.% NaCl is feed water and rpm is 3600.

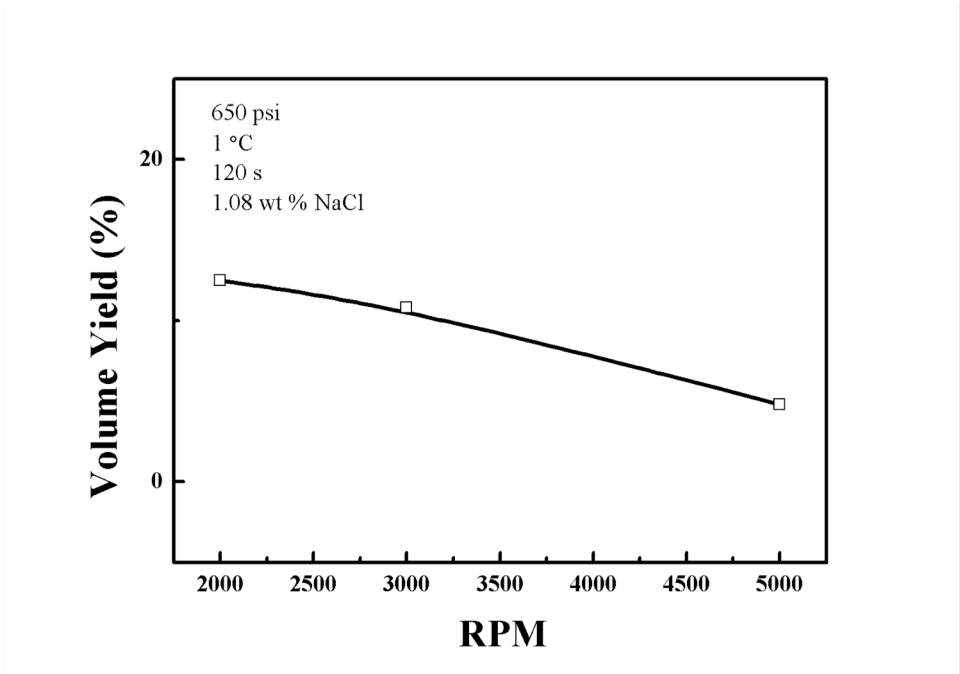

Figure 3.9 Effect of rpm effect on desalination volume, with initial pressure as 650psi and temperature as 1°C; 1.08wt.% NaCl is feed water and centrifuge time is 120s.

Dewatering by Filtration

We define the %Reduction of salt by following equation:

$$Desalination\ \%\ reduciton = \frac{c_1 - c_{product}}{c_1} \times 100\ \% \quad (3.14)$$

in which c_1 is the filtration feed water concentration; $c_{product}$ is the final solid hydrate product concentration.

Figure 3.10 shows effect of filtration time on %Reduction of NaCl. CO_2 hydrates were made at 1°C and 650psi. As shown, the %Reduction increased with increasing filtration time as anticipated. Also, the process is effective over a wide range of salinity, which is an advantage over reverse osmosis. We found that in the first region from 120 to 300s, %Reduction enhances rapidly from 52.53 to 97.14%. In the second region from 300 to 420s, %Reduction stays almost the same and changes between 97.14 and 98.43%. In the first region, longer filtration time results in more trapped in brine ions are released by melting, however, in the second region, we suggest that an attraction force may exist between salt ions and gas hydrate and begin to play the main role to obstruct removal of

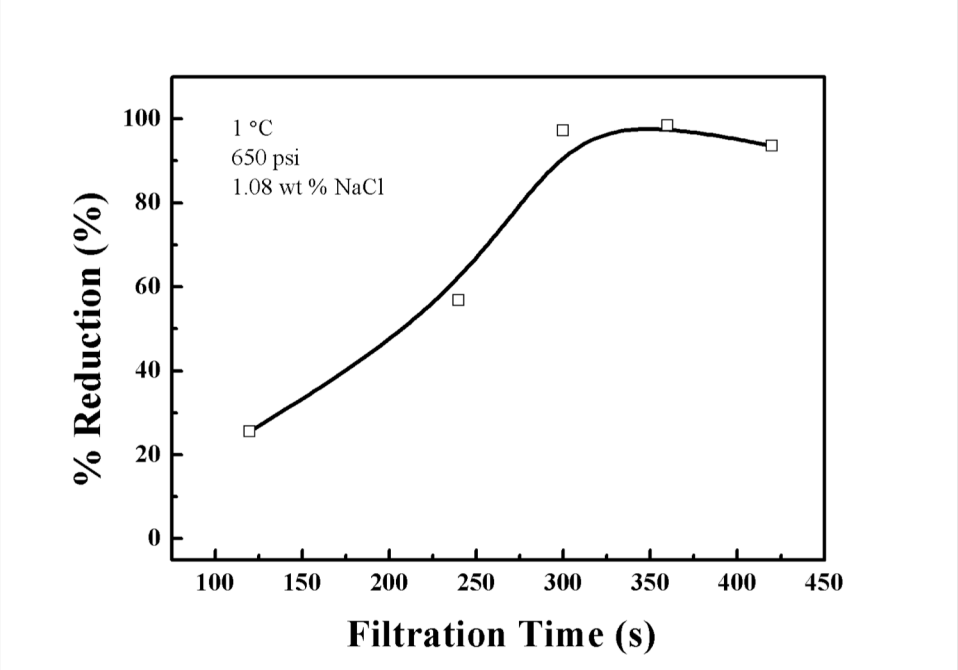

Figure 3.10 Effect of filtration time on %Reduction, with initial pressure as 650psi and temperature as 1°C; 1.08wt.% NaCl is feed water.

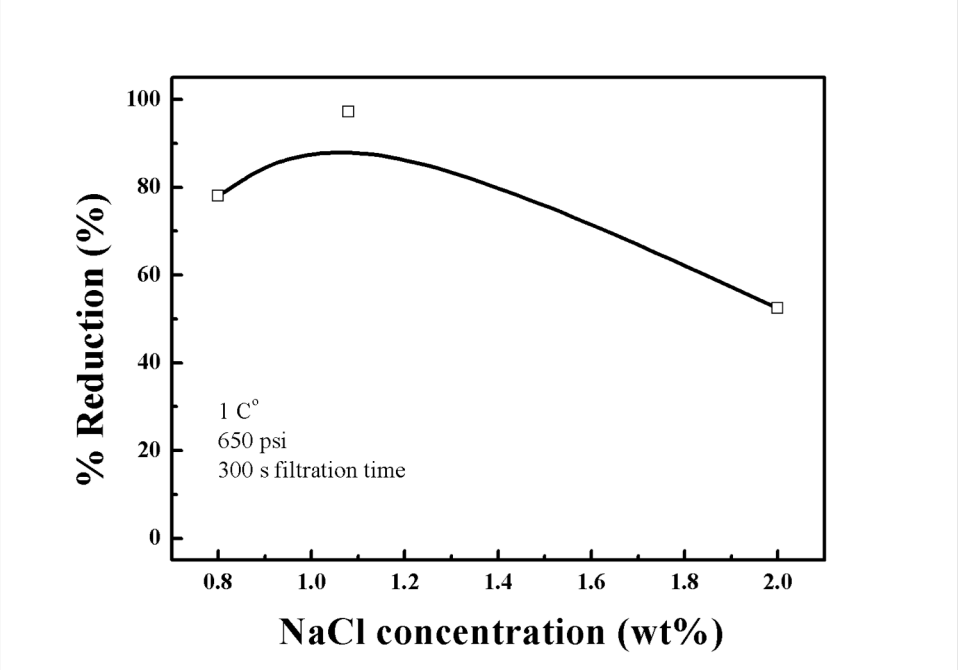

Figure 3.11 Effect of filtration time on %Reduction, with initial pressure as 650psi and temperature as 1°C; 1.08wt.% NaCl is feed water.

salinity.

We obtained three NaCl concentrations of 0.8, 1.08 and 2wt.% as feed water with consistent filtration time of 300s and CO_2 hydrate were formed under 650psi and 1°C. From **Figure 3.11**, an optimal concentration with the highest %Reduction of 98.42% is obtained and the concentration effect varies in different concentration ranges for NaCl. In Mohammad Sarshar [19] research, they prepared 1.5 to 3.0wt.% NaCl aqueous solution and obtained %Reduction varies from 3.3 to 52.0 % at 2.5 - 4.5MPa and 0 - 8°C in a 51 semi-batch reactor, and we obtained higher %Reduction than they did in the similar concentration range.

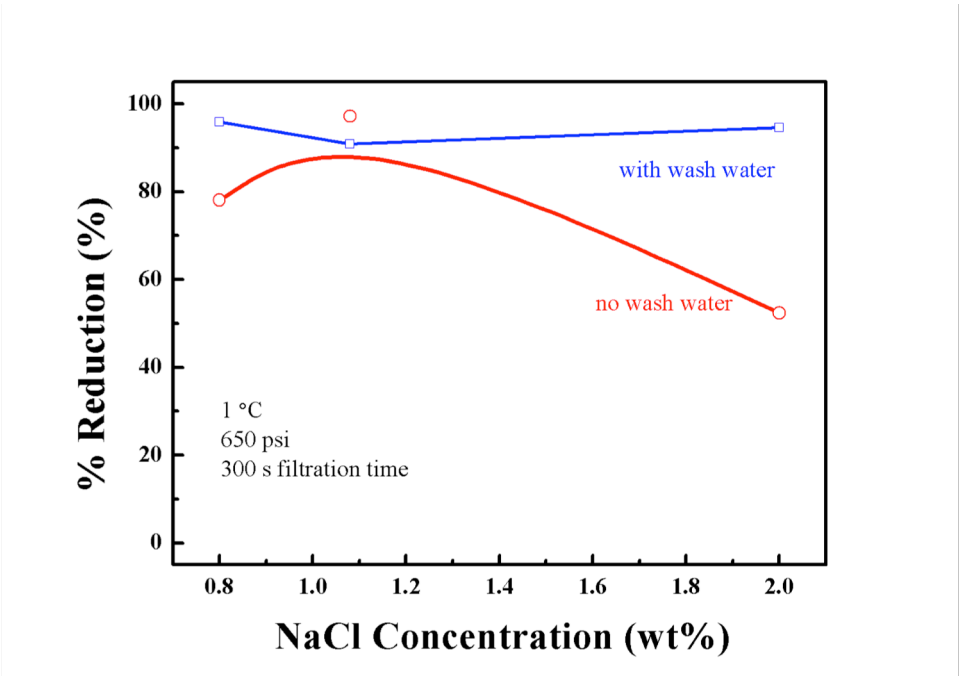

Figure 3.12 Effect of wash water on %Reduction in filtration, with initial pressure as 650 psi and temperature as 1°C; 1.08wt.% NaCl is feed water.

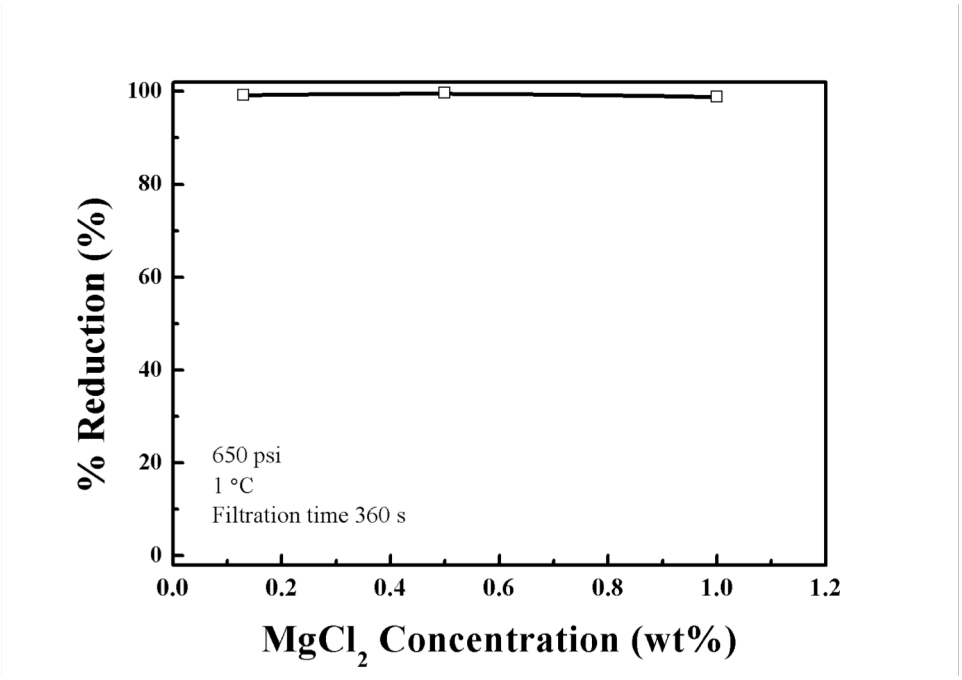

Figure 3.13 Effect of Mg^{2+} concentration on %Reduction in filtration, with initial pressure as 650psi and temperature as 1°C.

In industrial reverse osmosis desalination process, wash water composed of clean water is used to create high driving force. The impact of wash water was shown in **Figure 3.12**, adding wash water for 30 seconds leads to average %Reduction improved from 75.86 to 93.77%. But no proficient improvement of %Reduction with longer washing time was obtained. However, only 30s addition of wash water consumed 100 mL clean water, comparing to the small enhancement on the %Reduction, a more efficient and economic way need to be explored.

Figure 3.13 shows the results obtained with feed water as $MgCl_2$. Excellent results were obtained, which is showing over 99 %Reduction in the dissolved species. The effect of $MgCl_2$ concentrations is not obvious on the %Reduction, but an optimal concentration of 0.5 wt.% is obtained.

Comparing to the low %Reduction before filtration of 7.13%, it shows positive effect of filtration in desalination from Figure 3.14. We conclude that most part of salinity is removed in the filtration stage and gas hydrate formation prepares excellent gas hydrate feed to filtration in $MgCl_2$ solution desalination.

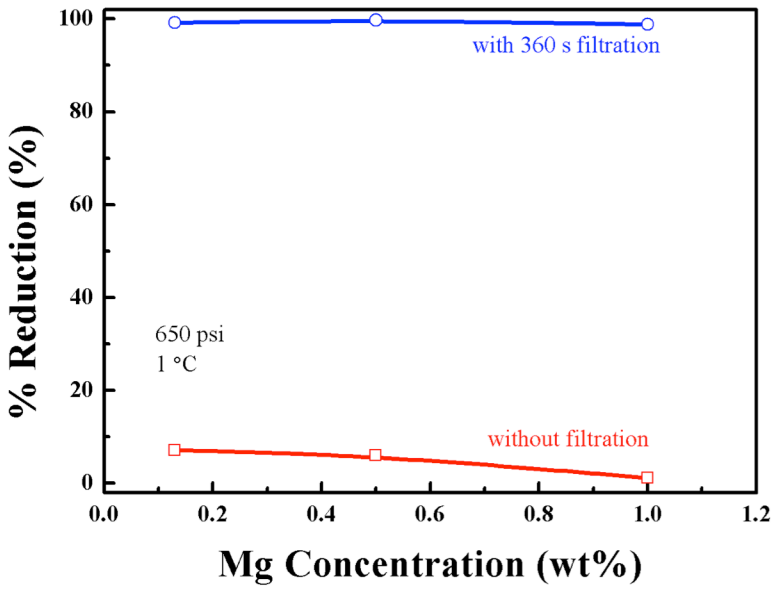

Figure 3.14 Comparison of Mg^{2+} concentration effect on %Reduction before and after filtration, with initial pressure as 650psi and temperature as 1°C.

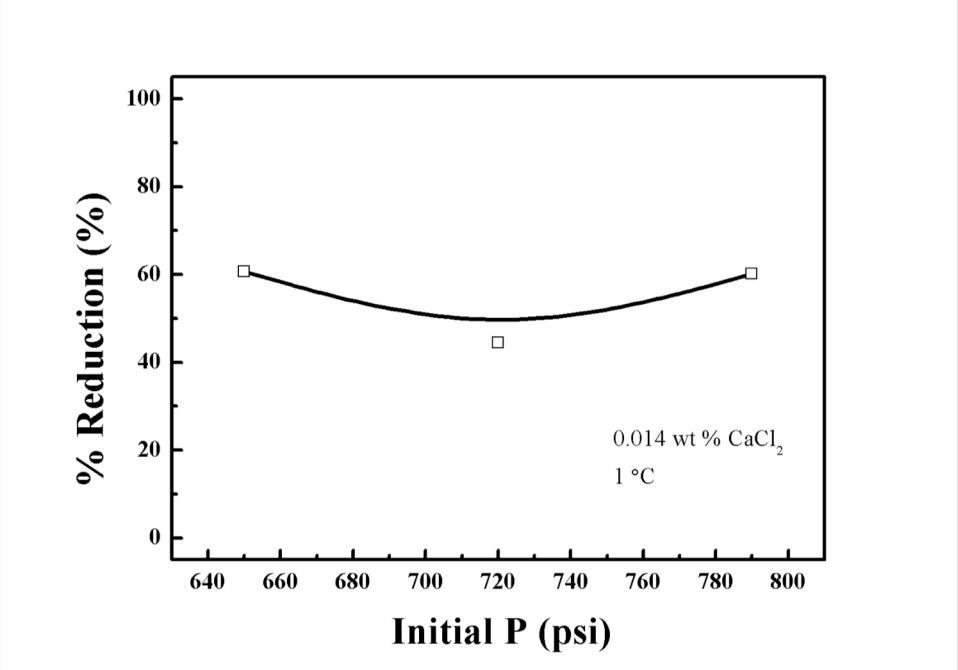

Figure 3.15 Effect of initial pressure on %Reduction in filtration, with 0.014wt.% $CaCl_2$ as feed water and initial temperature as 1°C.

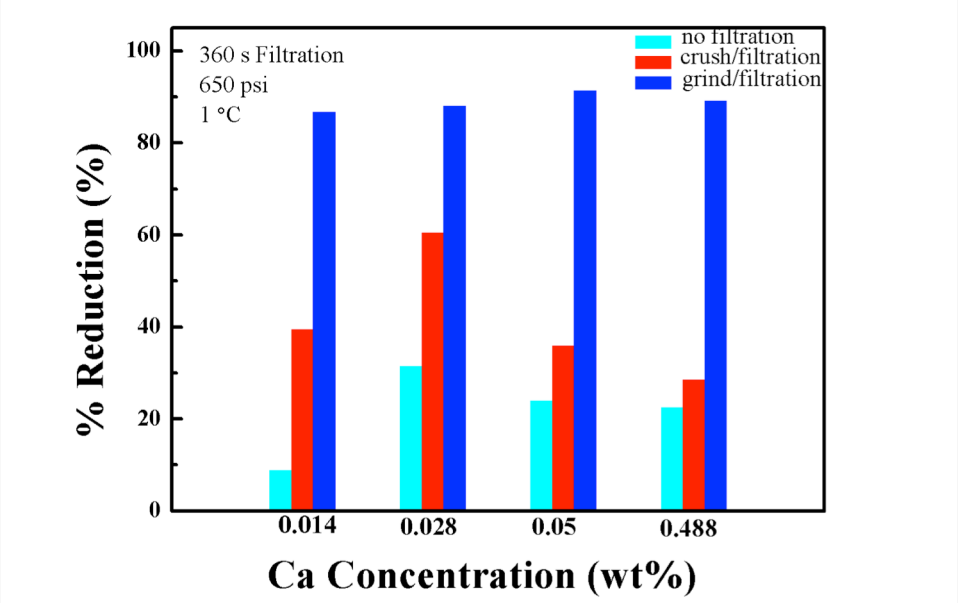

Figure 3.16 Effect of particle size and filtration on %Reduction of $CaCl_2$, with initial pressure as 650psi and temperature as 1°C.

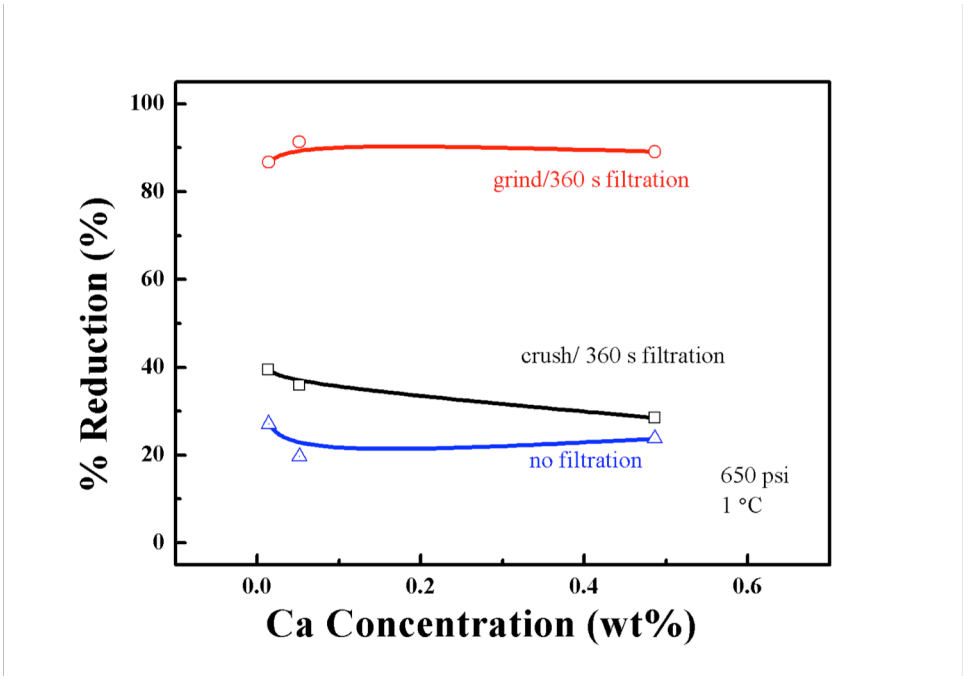

Figure 3.17 Effect of particle size and filtration on %Reduction of $CaCl_2$, with initial pressure as 650psi and temperature as 1°C.

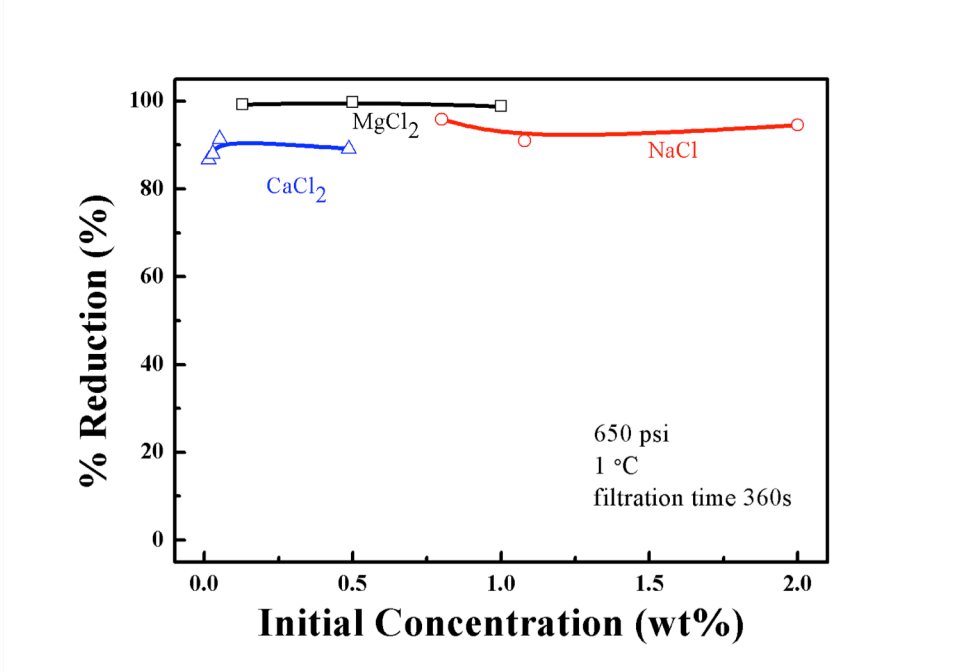

Figure 3.18 Effect comparison of artificial produced water with different TDS on %Reduction in filtration, with initial pressure as 650psi and temperature as 1°C, and filtration time is 360s.

In Figure 3.15, it indicates higher initial pressure doesn't remove more salinity with temperature as 1°C and 0.014wt.% $CaCl_2$ as feed water. So we control pressure as 650 psi in $CaCl_2$ desalination.

As shown in **Figure 3.16** and **Figure 3.17**, the %Reductions achieved without filtration were in the range of less than 20%. In the next series of experiments, the hydrate crystals were crushed and filtered. The %Reduction was increased considerably. After reducing the particle size further by grinding, %Reduction reached 90%, indicating that the finer the particle size, the higher the extent of cleaning.

In **Figure 3.18**, the result obtained with artificial produced waters containing $CaCl_2$, $MgCl_2$, and NaCl are plotted. These results demonstrate that the process we have developed could remove in excess of 90% of the dissolved solids. The highest average %Reduction of 99.23% was obtained in $MgCl_2$, the lowest was obtained in $CaCl_2$. We explained that Mg is easier to be sucked out of clathrate structure than other two ions due to the weakest connecting force with gas hydrate.

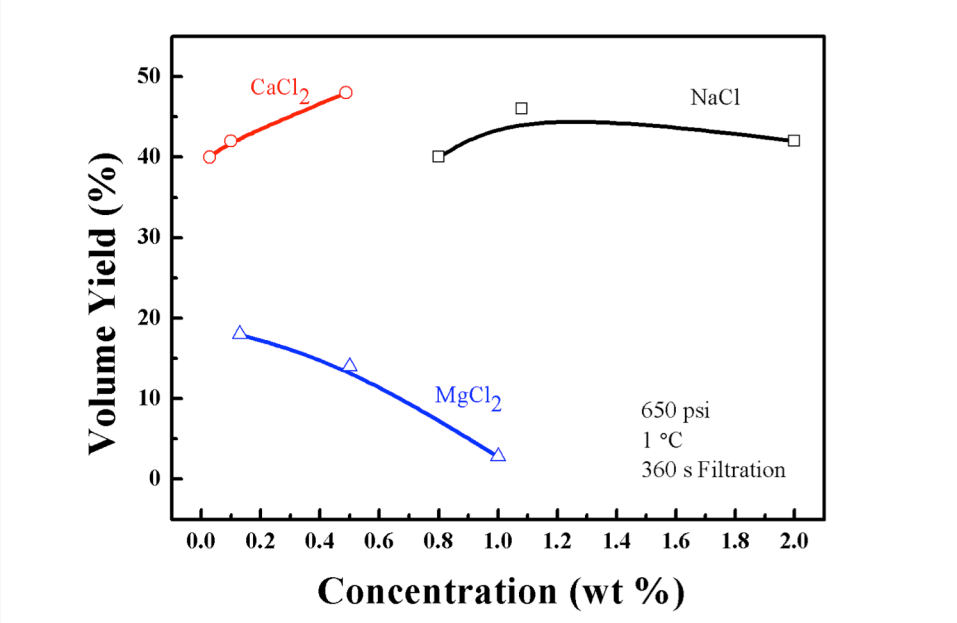

Figure 3.19 Effect comparison of artificial produced water of different TDS on desalination volume yield in filtration, with initial pressure as 650psi and temperature as 1°C, and filtration time is 360s.

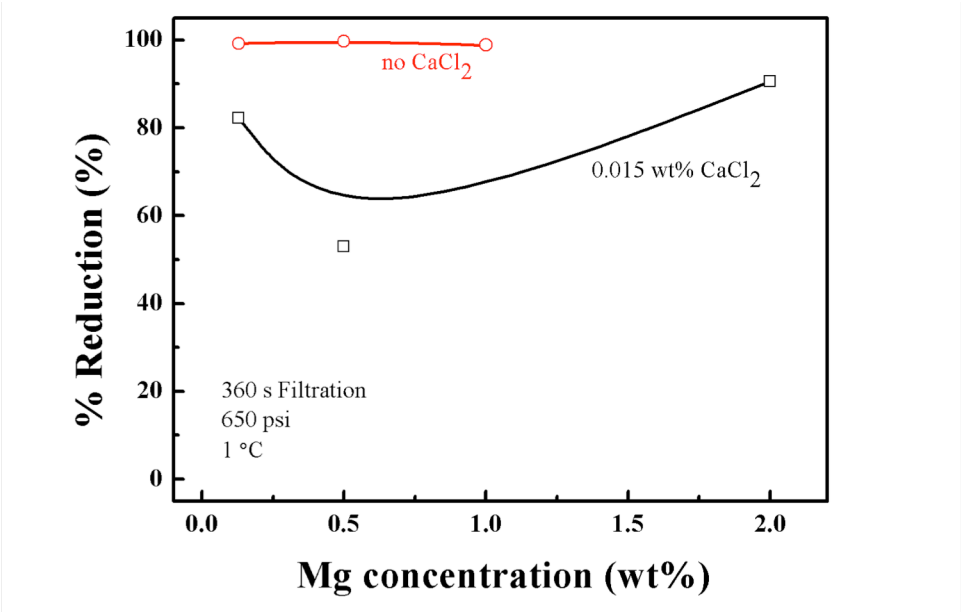

Figure 3.20 Effect of Mg^{2+} on the %Reduction in $MgCl_2$-$CaCl_2$ mixture in filtration, with initial pressure as 650psi and temperature as 1°C, and filtration time is 360s.

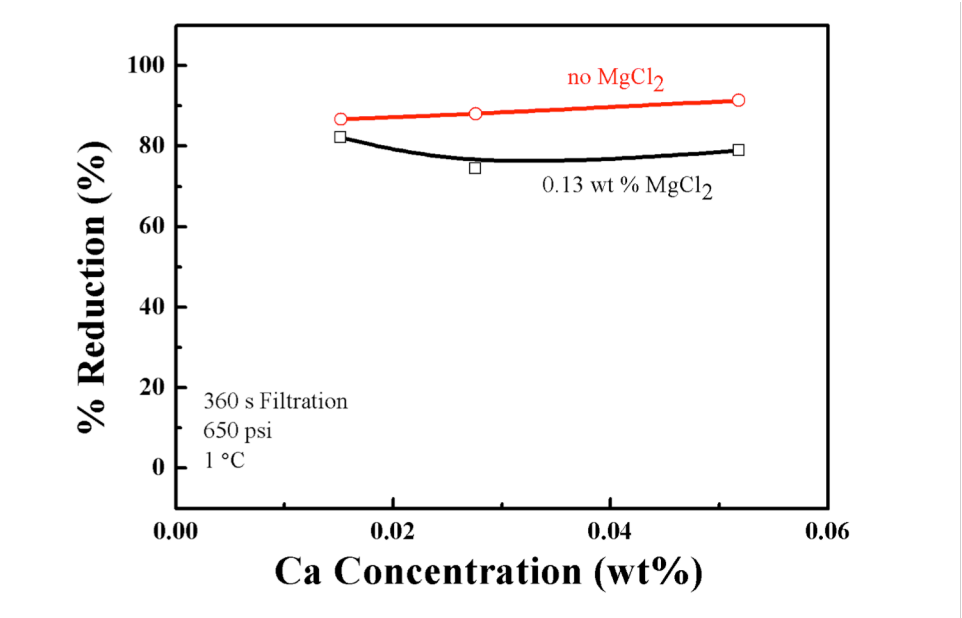

Figure 3.21 Effect of Ca^{2+} on the %Reduction in $MgCl_2$-$CaCl_2$ mixture in filtration, with initial pressure as 650psi and temperature as 1°C, and filtration time is 360s.

Volume yield are compared in **Figure 3.19**, $MgCl_2$ obtained the lowest volume yield, while $CaCl_2$ obtained the highest. We tried to explain from freezing point angle, NaCl

hydrate and $CaCl_2$ hydrate may have same freezing point that are both higher than that of $MgCl_2$ hydrate in experiments, and thus $MgCl_2$ hydrate melts in a faster speed. The volume yield relates to the %Reduction because of faster melting speed causes more brine ions to be released from clathrate structure.

In Ca-Mg mixture, Ca concentration was controlled as 0.015wt.% and Mg concentrations was controlled as 0.13 wt.% separately with results shown in **Figure 3.20** and **Figure 3.21**. It is obviously that addition of both $MgCl_2$ and $CaCl_2$ decrease %Reduction of salt comparing to corresponding single ion solution. The inhibiting effect of Ca is much stronger than that of Mg in mixture salinity removal. We assumed that calcium ions may connect with magnesium ion or with themselves more tight than magnesium ions connected with themselves.

Comparison between Centrifuge and Filtration

Comparison of %Reduction of salt between centrifuge and filtration is shown in **Figure 3.22**, it is easily to find out that filtration methods produces much higher %Reduction of 90 % than centrifugation does when 1.08 wt.% NaCl served as

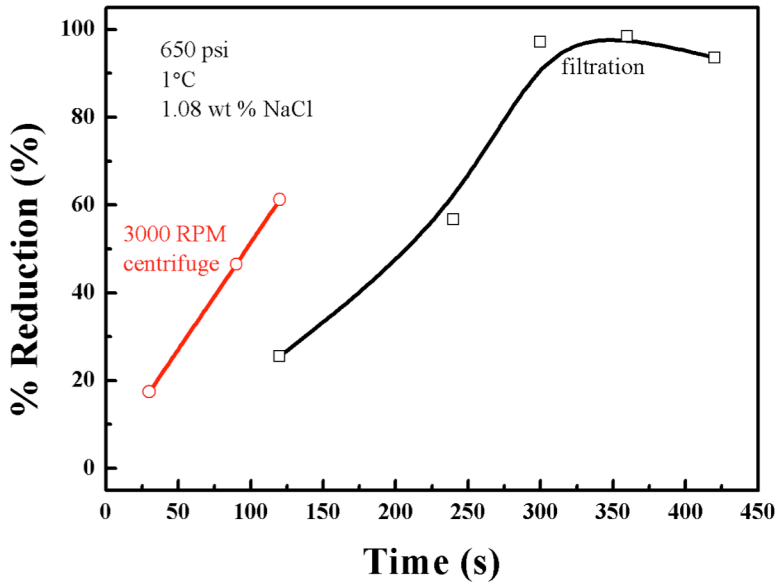

Figure 3.22 Effect comparison of centrifuge and filtration on %Reduction, with initial pressure as 650psi and temperature as 1°C, 1.08wt.% NaCl is feed water.

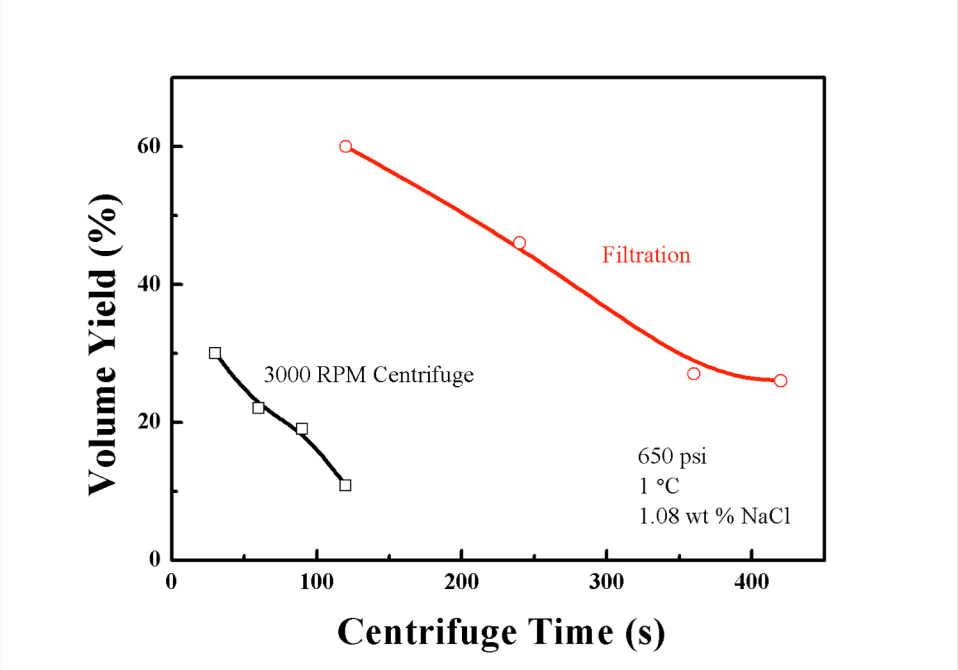

Figure 3.23 Effect comparison of centrifuge and filtration desalination volume yield, with initial pressure as 650psi and temperature as 1°C; 1.08wt.% NaCl is feed water.

feed water. However, filtration operates in longer time and thus more energy consumptions than centrifugation. If we performed two methods for same time period, e.g. centrifuge produces %Reduction of 61.25%, which is much higher than that of filtration in 120s separation. Overall, we assumed that increasing centrifuge time could remove more salinity of feed water.

The reason why we didn't centrifuge for long time was the low volume yield of centrifuge as shown in **Figure 3.23**. The volume yield of centrifuge decreases to as low as 10% for 120s, if we further increased centrifuge time, there may no solid gas hydrate product is obtained. The possible solution is that we operate centrifuge under lower temperature, such as in a cold room.

Process Flow Sheet

Based on the results presented above, we have developed a flow sheet for desalination of produced water, as shown in **Figure 3.24**. High salinity producer water is fed to a hydrate reactor using pressurized CO_2. The hydrate crystals will be fed to a screen to remove the water that has not been incorporated into hydrate as screen underflow. This water should have high concentrations of dissolved species such as Ca^{2+} and Mg^{2+} ions.

The hydrate crystals are recovered as screen overflow. These crystals are formed by pure water but contain some entrapped produced water in between the fine-grained crystals. In order to remove the entrapped produced water, the screen overflow is crushed, ground, and then subsequently dewatered using a centrifuge (or a filter). The dewatered CO_2 hydrate is melted down to clean liquid water. The clean water obtained in this manner should be free of dissolved species.

The filtrate from the dewatering centrifuge and the screen underflow are contacted with CO_2 to precipitate calcium and magnesium carbonate, which can be a byproduct that can be marketed as building materials, pigments, fillers, etc. The residual water from the CO_2 mineralization reactor will be fed to a flotation cell, in which air bubbles remove organic impurities. The underflow from the flotation column may be combined with the

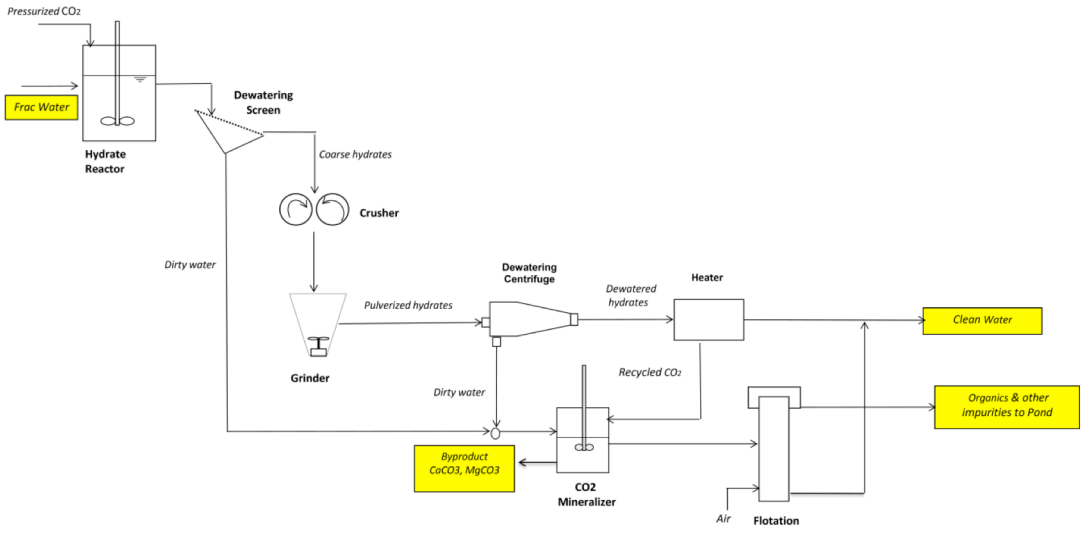

Figure 3.24 Process flow sheet for produced water desalination

clean water, while the overflow is sent to a pond.

Cost Analysis

In general, cost analysis is done on the basis of pilot- or full-scale tests. Since the results obtained to data are limited to small scale laboratory tests, we are presenting the

Table 3.5 Cost of reverse osmosis process for sea water desalination (El-Dessouky and Ettouney [1]).

Capital cost ($/1000 gal)		0.424
Operation cost ($/1000 gal)	Fixed charge	0.776
	Electricity	0.757
	Chemicals	0.125
	Membrane replacement	0.715
	Labor	0.189
	total	2.562
Total ($/1000 gal)		2.986

Table 3.6 Cost of hydrate crystallization process for seawater desalination. (McCormack and Niblock [5]).

	Public Financing		Private Financing	
	Capacity		Capacity	
	3.6 Mgal/day	7.2 Mgal/day	3.6 Mgal/day	7.2 Mgal/day
Capital cost ($/1000 gal)	0.88	0.83	1.44	1.33
Operation cost ($/1000 gal)	1.12	0.91	1.13	0.91
Total ($/1000 gal)	2.00	1.74	2.57	2.24

Table 3.7 Cost of multi-stage flash distillation process for sea water desalination. (El-Dessouky and Ettouney [2]).

Capital cost ($/1000 gal)		0.640
Operation cost ($/1000 gal)	Fixed charge	1.249
	Steam	1.526
	Electricity	0.946
	Chemicals	0.095
	Labor	0.378
	total	4.194
Total ($/1000 gal)		4.834

Table 3.8 Cost of reverse osmosis process for produced water desalination (Çakmakcı, et al. [4])

Capital cost ($/1000 gal)		4.694
Operation cost ($/1000 gal)	Fuel	4.921
	Pretreatment	4.353
	RO system	4.353
	Labor	1.325
	total	14.952
Total ($/1000 gal)		19.646

results of our comparative analysis as shown below.

Tables 3.5 to 3.7 show the costs of desalinating seawater suing three different processes, namely, reverse osmosis, distillation, and hydrate formation methods. The cost for desalinating 1,000 gallon of seawater decreases from $4.84 for multi-stage flash distillation, $2.98 for reverse osmosis, and $2.57 for hydrate formation. One can understand the fact that distillation is the most expensive of the three. However, it was surprising that the hydrate formation process was less costly than the reverse osmosis process despite the fact that Bradshaw et al. [20] used three-step hydrate formation process. The reason that they used the three-step process was because a single-step process was unable to remove sufficient amounts of salts due to the entrapment problem we have discussed in the present work.

We have shown in this report that the process of crushing and grinding followed by dewatering can reduce the multi-step hydrate formation process to a single-step process. Therefore, the process developed in the present work should substantially lower the cost of desalination below that reported by Bradshaw et al. [20]

As has already been noted, the reverse osmosis process has a serious problem in its application to desalinating produced water, particularly the frac water containing very high levels of TDS. For this reason, the cost of reverse osmosis increases sharply up to $19.6 per 1,000 gallons at high salinity as shown in Table 3.8. The process developed in the present work should be substantially lower than this figure. However, it is necessary to conduct a series of pilot-scale tests to carryout reliable cost analysis. The authors

believe that the process of desalinating produced water as described in this report is patentable.

3.4 Conclusions

The results obtained in this study showed that over 99% of dissolved NaCl and $MgCl_2$ can be removed from artificial saline water in a process involving a single-stage hydrate formation step, followed by a single-step dewatering (centrifugation or filtration). The results show that the %Reduction of NaCl increases with centrifugation time and rotational speed (rpm). Centrifugal filtration would have given better results for two reasons: *first*, the entrapped water removed by centrifugation was removed by decantation; therefore, part of the residual water still remained with the crystals. *Second*, the particle size of the broken hydrate crystals was too large. Crushing the crystals to finer sizes would have given better results.

The values of %Reduction of NaCl in filtration were substantially higher than obtained using the centrifugation. The % Reduction increased with increasing filtration time as anticipated. Also, the process is effective over a wide range of salinity, which is an advantage over reverse osmosis. Excellent results were obtained in $MgCl_2$, which is showing over 99% reduction in the dissolved species. In Ca-Mg mixture, Ca has stronger inhibiting effect than Mg on %Reduction.

In the next series of experiments, the hydrate crystals were crushed and filtered. The %Reduction was increased considerably. After reducing the particle size further by grinding, %Reduction reached 90%, indicating that the finer the particle size, the higher the extent of cleaning. These results demonstrate that the process we have developed can remove in excess of 90 % of the dissolved solids. The use of this new process should help minimize the steps involved in cleaning produced water.

3.5 References

1 El-Dessouky, H. T., Ettouney, H. M. . Fundamentals of salt water desalination. *Elsevier Science: Amsterdam, Netherlands* (2002).

2 Çakmakcı, M., Kayaalp, N., Koyuncu, I. . Desalination of produced water from oil production fields by membrane processes. *Desalination* **Vol. 222**, 176-186 ((2008)).

3 McCormack, R. A., Niblock, G. A. . Build and operate a clathrate desalination pilot plant, Final technical report, Thermal Energy Storage, Inc, Water Treatment Technology Program Report No. 31. *US Depart of Interior, Bureau of Reclamation* (1998).
4 Korsgaard, M. D. M. J. (2005, November).
5 Shannon, M. A. *et al.* Science and technology for water purification in the coming decades. *Nature* **452**, 301-310, doi:10.1038/nature06599 (2008).
6 Corak, D. *et al.* Effect of subcooling and amount of hydrate former on formation of cyclopentane hydrates in brine. *Desalination* **278**, 268-274, doi:10.1016/j.desal.2011.05.035 (2011).
7 Bozzo, A. T., Chen, H. S., Kass, J. R. & Barduhn, A. J. PROPERTIES OF HYDRATES OF CHLORINE AND CARBON-DIOXIDE. *Desalination* **16**, 303-320, doi:10.1016/s0011-9164(00)88004-2 (1975).
8 Jager, M. D. & Sloan, E. D. The effect of pressure on methane hydration in pure water and sodium chloride solutions. *Fluid Phase Equilib.* **185**, 89-99, doi:10.1016/s0378-3812(01)00459-9 (2001).
9 Ogienko, A. G., Manakov, A. Y., Kurnosov, A. V., Grachev, E. V. & Larionov, E. G. Direct measurement of stoichiometry of the structure H argon gas hydrate synthesized at high pressure. *J. Struct. Chem.* **46**, S65-S69, doi:10.1007/s10947-006-0153-7 (2005).
10 Atik, Z., Windmeier, C. & Oellrich, L. R. Experimental gas hydrate dissociation pressures for pure methane in aqueous solutions of MgCl2 and CaCl2 and for a (methane plus ethane) gas mixture in an aqueous solution of (NaCl+MgCl2). *J. Chem. Eng. Data* **51**, 1862-1867, doi:10.1021/je060225a (2006).
11 Bishnoi, P. R. & Dholabhai, P. D. EXPERIMENTAL-STUDY ON PROPANE HYDRATE EQUILIBRIUM CONDITIONS IN AQUEOUS-ELECTROLYTE SOLUTIONS. *Fluid Phase Equilib.* **83**, 455-462, doi:10.1016/0378-3812(93)87050-b (1993).
12 Aliev, A. M. *et al.* Mathematical modeling of seawater desalination by the gas hydrate method. *Theor. Found. Chem. Eng.* **45**, 185-189, doi:10.1134/s0040579511020023 (2011).
13 Veil, A., Puder, M.G., Elcock, D., Redweik, R.J.,Jr.,. A White Paprt Describing Produced Water from Production of Crude Oil, Natural Gas, and Coal Bed Methane. . (United States Department of Energy and National Energy Technology Laboratory, 2004).
14 Petroleum: Fossil Fuel Production. US Energy Information Administration: Independent Statistics and Analysis., (United States Department of Energy, 2010).
15 Jones, F. O. & Owens, W. W. A LABORATORY STUDY OF LOW-PERMEABILITY GAS SANDS. *J. Pet. Technol.* **32**, 1631-1640 (1980).
16 Jones, A. H., Bell, G.J., Schraufngel, R.A.,. A review of the physical and mechanical properties of coal with implications for coalbed methane well completion and production: coalbed merhane, San Juan Basin. . (Rockey Mountain Association of Geologists, 1988).
17 Curtis, J. B. Fractured shale-gas systems. *AAPG Bull.* **86**, 1921-1938 (2002).
18 Alley, B., Beebe, A., Rodgers, J. & Castle, J. W. Chemical and physical characterization of produced waters from conventional and unconventional fossil

fuel resources. *Chemosphere* **85**, 74-82, doi:10.1016/j.chemosphere.2011.05.043 (2011).

19 Sarshar, M. & Sharafi, A. H. Simultaneous water desalination and CO(2) capturing by hydrate formation. *Desalin. Water Treat.* **28**, 59-64, doi:10.5004/dwt.2011.2201 (2011).

20 Bradshaw, R., Greathouse, J. A., Cygan, R. T., Simmons, B. A., Dedrick, D. E., Majzoub, E. H. . Desalination Utilizing Clathrate Hydrates (LDRD Final Report). *Sandia National Laboratory* ((2008)).

Chapter 4 Conclusion and Future Work

4.1 Conclusion

The results obtained in this study showed that over 99% of dissolved NaCl and $MgCl_2$ can be removed from artificial produced water in laboratory experiments. This was achieved in a process involving a single-stage hydrate formation step, followed by a single-step solid-liquid separation (or dewatering).

1) The CO_2 consumption for the removal of both $MgCl_2$ and $CaCl_2$ is much lower than that for the removal of NaCl.
2) There is no correlation between the TDS of artificial produced water and the induction time.
3) The results show that the %Reduction of NaCl increases with centrifugation time and rotational speed (rpm). The removal efficiency with increasing rpm is due to the increase in the G-force.
4) The %Reduction of NaCl achieved by filtration was substantially larger than achieved by centrifugation. The %Reduction increased with increasing filtration time as anticipated.
5) The %Reduction of $MgCl_2$ was over 99% after filtration.
6) The %Reduction of $CaCl_2$ increased substantially after the hydrate crystals were crushed and filtered. After reducing the particle size further by grinding, %Reduction reached 90%, indicating that the finer the particle size, the higher the extent of cleaning.
7) The concentration range of TDS that can be handled by this process is much larger than the range at which reverse osmosis can be used. Thus, the use of this new process should help minimize the steps involved in for removing TDS from produced water.

4.2 Future Work

1) Perform centrifugation process in cold room to modify the melting problem of gas hydrate to achieve higher water recovery.
2) Scale-up the process for possible commercialization.